1 Abstract

This document examines the Underlying Flow Regime of a turbulent, non-reacting plume flowing into a quiescent and unstratified environment. Only the unsteady flow behaviour in the near-field is considered, within the region extending up to around five diameters downstream from the source. Figure 1 shows a CFD simulation of such a plume. The fully-developed, far-field behaviour of turbulent plumes is examined in a related UFR.

Turbulent buoyant plumes are a feature of many important scientific and engineering applications including flows generated by fires, smokestacks, cooling towers, and large geothermal events, such as volcanoes. The source of the buoyancy may be provided by temperature differences in the fluid or can be related to two fluids of different density mixing together.

Medium to large scale plumes are characterised by the repetitive shedding of coherent vortical structures at a well-defined frequency, a phenomenon known as “puffing”. A number of empirical correlations for the puffing frequency of plumes have been developed, based on the Richardson number, which are described in this UFR.

A brief review is provided of near-field plume experiments and CFD studies. Three CFD studies are examined in greater detail, those by DesJardin *et al*. [1], Tieszen *et al*. [2] and Xin [3]. These have all simulated the recent helium plume experiments of O'Hern *et al*. [4]. The studies have each used slightly different numerical modelling approaches, although all are based on Large-Eddy Simulation (LES). The plume experiments O'Hern *et al*. [4] are particularly well-suited for model evaluation as they involved simultaneous measurement of velocities and mass fraction, allowing both Reynolds and Favre-averaged quantities to be determined.

Based on the three CFD studies, best practice advice is provided for industrial CFD practitioners on some key modelling issues involved in simulating unsteady buoyant plumes.

LES is less mature than RANS turbulence modelling and a number of uncertainties remain when using LES for industrial flow predictions, such as the appropriate grid resolution and the choice of numerical schemes. Some guidance is given on these issues and suggestions are provided for where future work could contribute to providing improved quality and trust in the simulation of plumes.

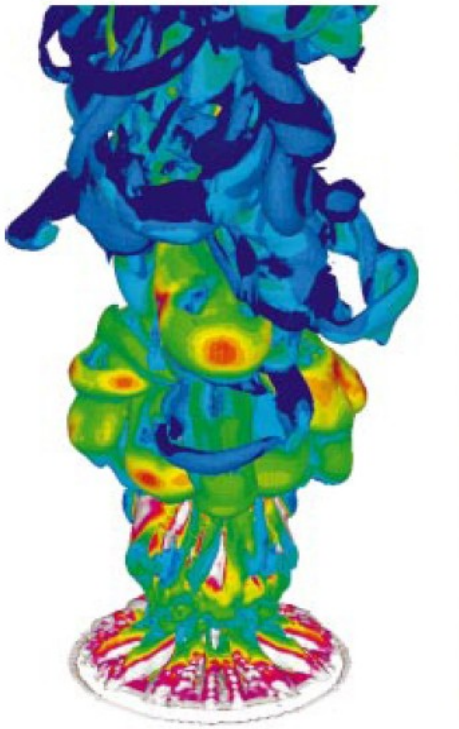

Figure 1 CFD Simulation of the near-field of a buoyant helium plume. The vorticity iso-surface is coloured with the magnitude of the gravitational torque. From DesJardin *et al*. [1]

2 Description

2.1 Introduction

Free vertical buoyant plumes and free-jets are related phenomena, both having a core region of higher momentum flow surrounded by shear layers bounding regions of quiescent fluid. However, whereas for jets the driving force for the fluid motion is a pressure drop through an orifice, for plumes the driving force is buoyancy due to gradients in fluid density. Plumes can develop due to density gradients caused by temperature differences, for example in fires, or can be generated by fluids of different density mixing, such as hydrogen releases in air. There are many flows of both engineering and environmental importance that feature buoyant plumes, ranging from flows in cooling towers and heat exchangers to large geothermal events such as volcanic eruptions. There has been considerable attention paid to the mean flow behaviour of plumes in the far field, e.g. Chen & Rodi [5] or List [6][7], which are examined in a companion UFR. However, there has been less study of the near-field unsteady dynamics of plumes.

In the present work, only non-reacting plumes are considered. This choice has been made in order to avoid the additional complexities associated with combustion, soot production and radiation in fire plumes. For helium plumes, the difference in density between helium and air is a factor of seven which is similar to that in fire plumes [8]. The principal difference between fire and helium plumes arises from the fact that heat is released locally from the flame in fire plumes whereas in helium plumes the buoyancy is produced only near the source where there are large concentration gradients.

The near-field of buoyant plumes features two key instabilities. The first is the Rayleigh-Taylor instability related to the presence of dense fluid above less-dense fluid. The two layers of different-density fluid are in equilibrium if they remain completely plane-parallel but the slightest disturbance causes the heavier fluid to move downwards under gravity through the lighter fluid. At the interface between the two fluids, irregularities are magnified to form fingers or spikes of dense fluid separated by bubbles of lighter fluid. The size of these irregularities grows exponentially with time and the smaller the density difference, the larger the wavelength of the instability. There has been considerable research into the dynamics of Rayleigh-Taylor instability (e.g. [9][10][11][12]) as a consequence of its importance in nuclear weapons, atmospheric flows and astrophysics. Figure 2 shows the classic spike and bubble flow structures characteristic of R-T instability produced by two fluids of different density mixing, taken from Cook *et al*. [13].

Figure 2 Rayleigh-Taylor instability, from Cook *et al*. [13]. The heavy fluid is in black.

The second instability in buoyant plumes is the Kelvin-Helmholtz instability related to the shear-layer interface between the rising plume and the ambient fluid. This forms axisymmetric roll-up vortex sheets on the boundary between the two layers of fluid travelling at different velocities, and is a feature in practically all turbulent shear flows including jets and wakes.

There is some uncertainty over the relative significance of the R-T and K-H instabilities in buoyant plumes. Buckmaster & Peters [14], Ghoniem *et al*. [15], Coats [16], and Albers & Agrawal [17] have suggested that the K-H instability plays the dominant role in plumes whilst others, including DesJardin *et al*. [1], Tieszen *et al*. [2] and Cetegen & Kasper [18], suggest that the R-T instability is more important. For more details of the instability mechanisms and the transition to turbulence in buoyant flows, see also Gebhart *et al*. [19].

The Puffing Cycle

Medium to large scale plumes are characterised by the repetitive shedding of coherent vortical structures at a well-defined frequency, a phenomenon known as "puffing". DesJardin *et al*. [1] present a detailed analysis of the plume puffing cycle, which they decompose into a number of stages. In the first stage, the less-dense plume fluid is rising close to the plume axis. Near the base of the plume, there is a layer of dense air overlying the less-dense plume fluid. There are two instabilities near the edge of the plume: one related to the misalignment of the vertical pressure-gradient and radial density gradient (the baroclinic torque) and another due to the misalignment of the vertical gravity and the radial density gradient (the gravitational torque). These produce a rotational moment on the fluid, increasing its vorticity and pulling air into the plume. The fluid motion coalesces to produce a large toroidal vortex which is self-propagated vertically upwards. As the vortex shifts vertically, fluid is pumped through to the core of the plume resulting in higher velocities on the plume axis. Radial velocities are induced near the base of the plume and air is drawn in producing an unstable stratification of denser fluid above less-dense fluid, ready for the cycle to begin again.

Using Direct Numerical Simulation (DNS), Jiang & Luo [20][21] found that the gravitational torque is responsible for much of the initial production of vorticity in plumes. The term is highest towards the edge of the plume where the density gradient vector is pointing radially outwards at right-angles to the gravitational vector. The baroclinic torque was found to dominate the vorticity transport once the puffing structure has been established.

The toroidal vortex structure produced in small puffing plumes of helium in air, with a source

diameter of under 10 cm, is relatively coherent. As the size of the plume is increased, the strength of secondary azimuthal instabilities increase which destabilize the toroidal vortex, producing finger-like instabilities. These are shown clearly near the base of the plume in the LES of DesJardin *et al*. [1] (see Figure 3). The secondary instabilities generate streamwise vorticity that enhances the mixing process. DesJardin *et al*. suggest that capturing these instabilities may be important in numerical simulations of pool fires where combustion is predominantly mixing-controlled.

Figure 3 An instantaneous snapshot of the puff cycle from DesJardin *et al*. [1] showing the finger-like azimuthal instabilities near the base of the plume. The isocontour of streamwise vorticity is shown at ±10% of the peak value.

Characteristic Dimensionless Parameters

There are a number of dimensionless parameters which are used to characterise buoyant plumes. For plumes produced by a release of buoyant gas, the inlet Reynolds number, *Re*, is given by:

$$Re = \frac{\rho_0 V_0 D}{\mu} \tag{1}$$

where ρ_0 is the plume fluid density, V_0 is the inlet velocity, D is the characteristic inlet length scale or inlet diameter and μ is the dynamic viscosity. The Reynolds number represents the ratio of inertial forces to viscous forces. At high Reynolds numbers, the destabilizing inertial forces dominate the viscous forces and the flow is turbulent. For isothermal pipe flows, this occurs for $Re > 3000$. Between $2000 < Re < 3000$ the flow is transitional for $Re < 2000$ the flow is usually laminar.

A useful parameter for describing buoyant flows is the densimetric Froude number, *Fr*, which represents the ratio of inertial forces to buoyancy forces. It is defined here as:

$$Fr = \frac{V_0}{\sqrt{g\,D\left(\rho_\infty - \rho_0\right)/\rho_\infty}} \tag{2}$$

where g is the gravitational acceleration and ρ_∞ is the ambient fluid density. The densimetric Froude number varies from near zero for pure plumes to infinity for pure jets. Some texts choose to define Fr using the square of the definition given above (e.g. Chen & Rodi [5]).

The Richardson number, Ri, is simply the inverse of the square of the Froude number:

$$Ri = \frac{\left(\rho_\infty - \rho_0\right) g\, D}{\left(\rho_\infty V_0^2\right)} \tag{3}$$

In some texts, the density difference in the Froude and Richardson numbers is made dimensionless using the plume source density, ρ_0, instead of the ambient density, ρ_∞.

Subbarao & Cantwell [22] note that the Richardson number can be interpreted as the ratio of two timescales: the time for a fluid element to move one jet diameter due to inertia, $\tau_1 = D/V_0$, and the time for a fluid element to move the same distance under the action of buoyancy, $\tau_2 = \left[\rho_\infty D/g\left(\rho_\infty - \rho_0\right)\right]^{1/2}$, where:

$$Ri = \left(\frac{\tau_1}{\tau_2}\right)^2 \tag{4}$$

In addition to Reynolds-number effects, the transition from laminar to turbulent flow is affected by the strength of buoyancy. In a buoyant plume that is initially laminar but transitions to turbulent flow at some distance further downstream, the point at which transition occurs moves closer to the source as either the Reynolds number or the Richardson number is increased [22].

Frequency of Pulsatile Plume Motion

The dimensionless Strouhal number, St, is used to describe the oscillation frequency of unsteady plumes. It is defined as follows:

$$St = \frac{f\,D}{V_0} \tag{5}$$

where f is the frequency of the oscillation.

A number of empirical correlations for the puffing frequency of plumes have been developed based on the Richardson number. Cetegen & Kaspar [18] found that for axisymmetric helium-air plumes with $Ri < 100$, the Strouhal number was related to the Richardson number by:

$$St = 0.8\,Ri^{0.38} \tag{6}$$

The graph of St versus Ri taken from their paper showing this relationship is reproduced in Figure 4. Between $100 < Ri < 500$ there is a transitional region as the plume becomes more turbulent and

mixing is enhanced. For $Ri > 500$ the Strouhal number was found to scale according to:

$$St \propto Ri^{0.28} \tag{7}$$

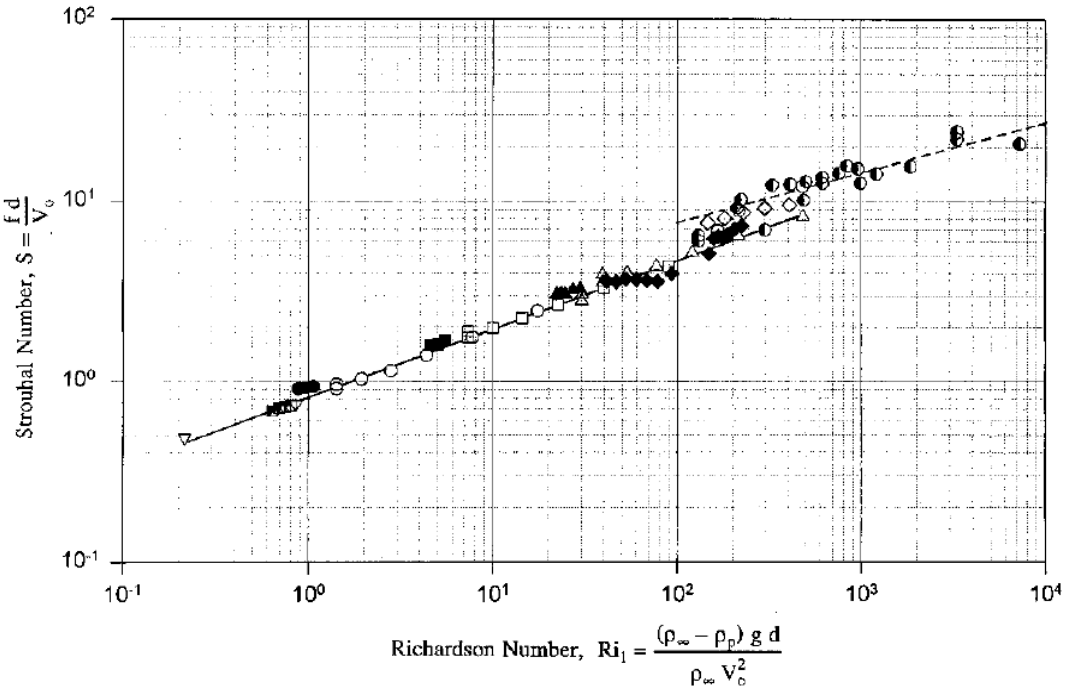

Figure 4 Correlation of puffing frequency in terms of Strouhal number and modified Richardson number for axisymmetric helium plumes, from Cetegen & Kaspar [18].

For planar helium plumes (produced by rectangular nozzles) with Richardson number in the range $1 < Ri < 100$, Cetegen *et al*. [23] found that the Strouhal number varied according to:

$$St = 0.55\, Ri^{0.45} \tag{8}$$

A similar relationship for planar plumes was obtained in the more recent DNS of planar plumes by Soteriou *et al*. [24], who obtained the correlation:

$$St = 0.536\, Ri^{0.457} \tag{9}$$

The difference between the puffing frequency in planar and axisymmetric plumes has been attributed to the difference in mixing rates and the strength of the buoyancy flux in the two cases. If the planar and axisymmetric Strouhal number correlations given by Equations (6) and (8) are extrapolated to higher Richardson numbers, they suggest that planar plumes exhibit higher frequency pulsations for $Ri > 211$ (where the two correlations cross over).

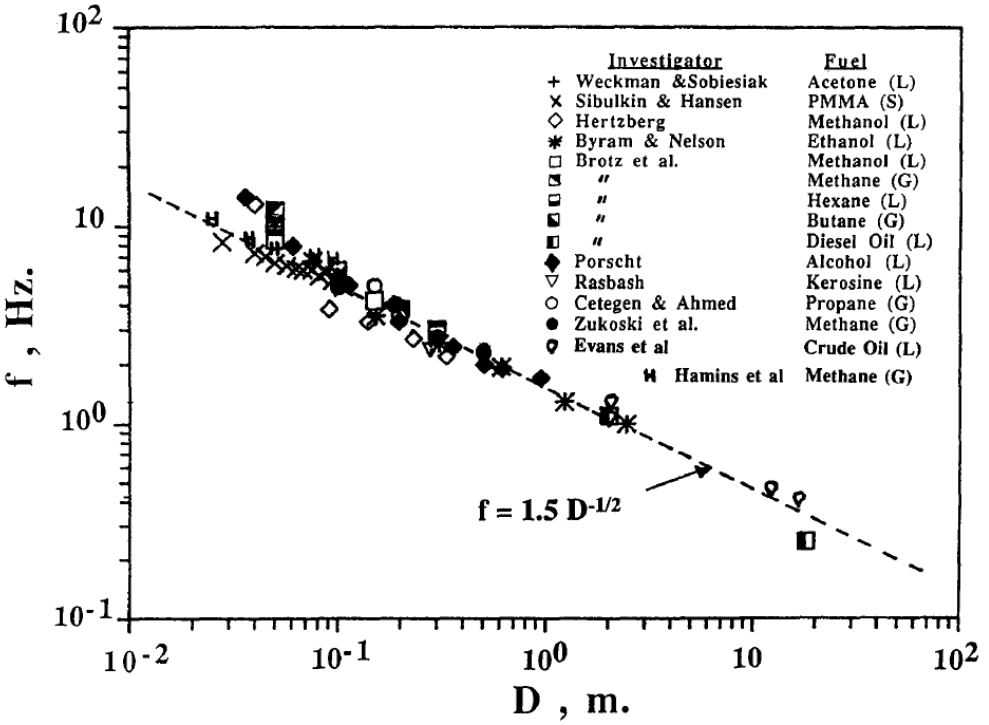

Figure 5 Puffing frequency of pool fires as a function of the burner diameter, *D*, from Cetegen & Ahmed [25].

For axisymmetric fire plumes, Cetegen & Ahmed [25] found the following relationship between the puffing frequency, *f*, and the diameter of the burner or source, *D*:

$$f = 1.5\, D^{-1/2} \tag{10}$$

Their correlation is compared to the experimental data in Figure 5. It is remarkably consistent, considering that the fire plumes used in their study involved solid, liquid and gas fuel sources. The dependence of the puffing frequency on the source diameter is slightly stronger in helium plumes, where $f \propto D^{-0.62}$ [18]. For planar helium plumes, Soteriou *et al*. [24] showed that the frequency varied according to $f \approx 0.5\sqrt{g/D}$.

Observations from plume experiments [18][22][26] and CFD simulations [24] have shown that the pulsation frequency in plumes does not strongly depend on the Reynolds number. The relative unimportance of the Reynolds number suggests that the instability mechanism controlling the pulsatile behaviour is essentially inviscid [24]. Once the conditions are met for the plume to become oscillatory, viscosity no longer appears to play a significant role in the puffing frequency. The helium plume experiments and simulations reported by Soteriou *et al*. [24] showed that the puffing frequency is unaffected by having the nozzle orifice flush to a solid surface or having the pipe from which the buoyant fluid escapes mounted free from the surrounding walls.

Onset of Pulsatile Flow Behaviour

The onset of unsteady flow behaviour in plumes is controlled by the balance of inertial, viscous and buoyancy forces. When viscous forces dominate, the plume remains steady.

Cetegen *et al*. [23] and Soteriou *et al*. [24] investigated in depth the transition from steady to unsteady flow behaviour in planar non-reacting plumes using both experiments and direct numerical simulation. Figure 6a shows some of their results, where plumes are characterised as either stable or unstable. The graph axes are the source Reynolds number and the inverse density ratio, $1/S = \rho_0/\rho_\infty$. Clearly, as either the Reynolds number is increased or the inverse density ratio decreases, the plume becomes less stable.

Experiments with both axisymmetric and planar plumes have found that pulsations are not produced when the density ratio exceeds $\rho_0/\rho_\infty \approx 0.6$ [18][23][27][28]. Simulations by Soteriou *et al*. [24] showed that pulsations could in fact be produced at density ratios closer to one, but that the Froude and Reynolds numbers at which these pulsations were obtained would not be easily achieved experimentally.

Using their simulations, Soteriou *et al*. [24] were able to examine separately the effects of the Reynolds number, the density ratio and the Froude number on the onset of transition. They obtained a transition relationship between Reynolds and Richardson numbers of $Re = 183\, Ri^{-0.627}$ (see Figure 7). The plume was unsteady for Reynolds or Richardson numbers above the line shown in the graph (i.e. for $Re > 183\, Ri^{-0.627}$ or $Ri > (Re/183)^{0.627}$).

Cetegen *et al.* [23] showed experimentally that when the nozzle orifice is mounted flush to a wall, the transition from a stable to an oscillatory plume occurs at a lower threshold velocity. The presence of a flat plate surrounding the nozzle prevents any coflow which results in higher induced cross-stream velocities. These cause the plume immediately downstream of the nozzle to contract more and produce a thinner column of buoyant fluid that is more susceptible to perturbations.

In terms of the onset of unsteady flow behaviour, axisymmetric plumes are significantly more stable than planar plumes. This is shown clearly in the results of Cetegen *et al*. [23] (Figure 6b), where the conditions for stability of axisymmetric plumes are shown in addition to the planar plume behaviour with and without a flat plate.

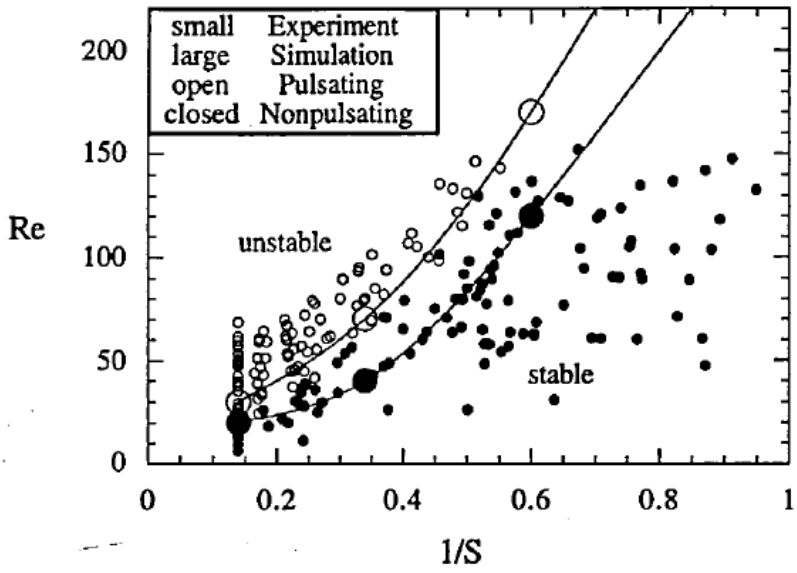

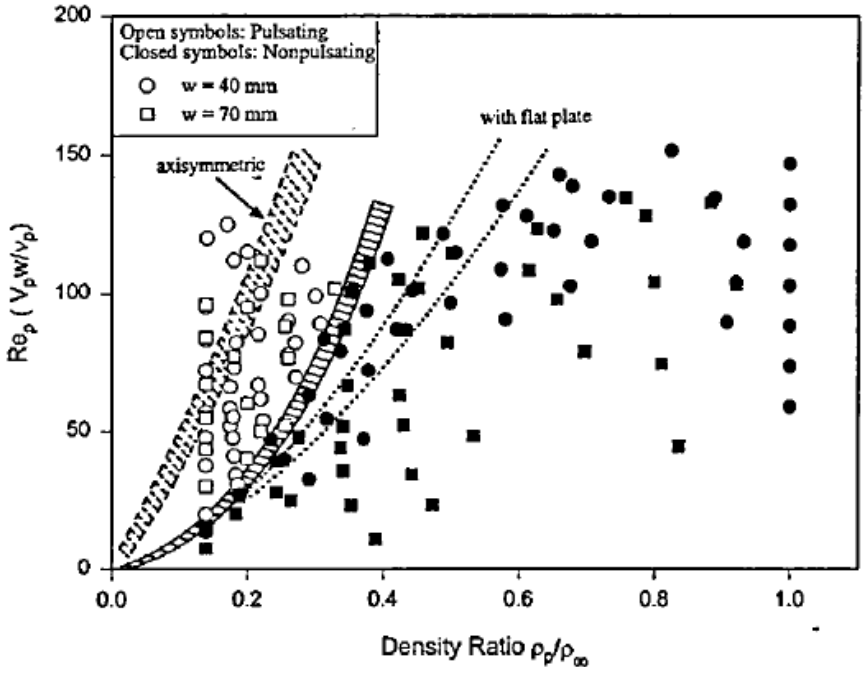

Figure 6 Stability of buoyant plumes for different density ratios and Reynolds numbers: a.) experimental and DNS results for planar plumes from Soteriou *et al*. [24] (top); b.) experimental results for planar and axisymmetric plumes with and without a flat plate around the nozzle from Cetegen *et al*. [23] (bottom).

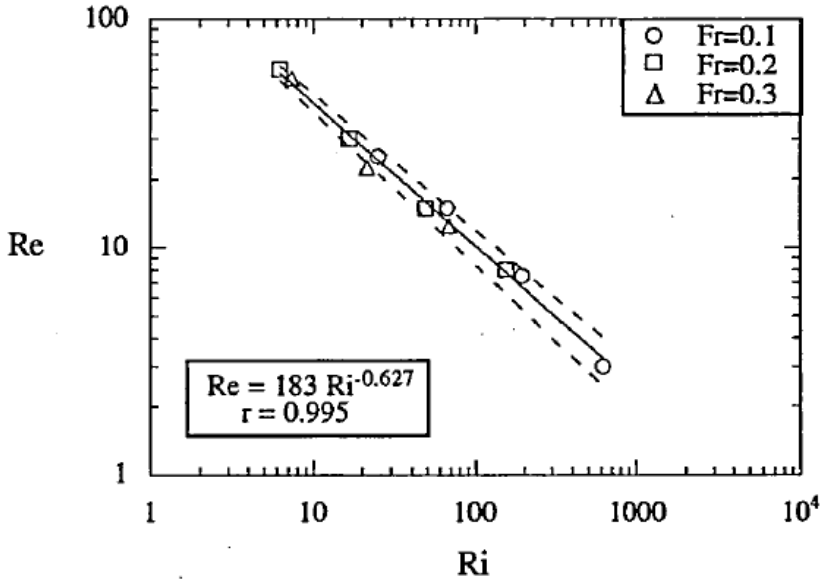

Figure 7 Transition from laminar to turbulent flow in planar plumes as a function of the Reynolds and Richardson numbers, from the DNS of Soteriou *et al*. [24]. Symbols indicate the results from simulations and the solid line is a fit to the data.

2.2 Review of UFR Studies and Choice of Test Case

Experiments

Most of the experimental data available on the near-field unsteady behaviour of non-reacting buoyant plumes has originated from the following American groups:

- Cetegen *et al*. (University of Connecticut) [18][23][24][28][29][30]
- Mell *et al*. (National Institute for Standards & Technology, NIST) [31][32]
- Subbarao & Cantwell (Stanford University) [22]
- Agrawal *et al*. (University of Oklahoma/NASA) [33][34]
- Gebhart *et al*. (Cornell University) [19][35][36]
- O'Hern *et al*. (Sandia National Laboratories) [4][37]

Cetegen *et al*.'s group examined both reacting and non-reacting plumes over a period of nearly a decade. Over that time, a number of significant works were published on axisymmetric helium plumes [18][30], planar helium plumes [23] and the effect of acoustic forcing on helium plumes [28][29]. A website with animations of various plumes is also online[1]. Empirical correlations were produced for the puffing frequency of planar and axisymmetric plumes and the causes of transition from steady to oscillatory plume behaviour were investigated (see discussion above). Their work on forced plumes involved using a loudspeaker to impart streamwise velocity fluctuations to the plume fluid. They found that plumes responded readily to the forcing and produced toroidal vortices at the forcing frequency. Interestingly, as the forcing approached the natural frequency of the flow, the large-scale vortices became more unstable and chaotic. This contrasts to other flows, such as jets

1 http://www.engr.uconn.edu/~cetegen/cetegen/previous%20research/researchproj.html?plume

and mixing layers, where forcing at the natural frequency leads to more spatial and temporal coherence.

In 1994, a series of helium plume experiments were undertaken by Johnson at NIST. Pure helium was released vertically through a 7.29 cm diameter pipe into ambient, quiescent air. The exit velocity was varied to examine different conditions and simultaneous velocity and concentration measurements were made. The data from these experiments has never been published fully in a conference or journal paper, but it has been used in two published computational studies by Mell *et al*. (also at NIST) [31][32]. The full data is also now available online on Mell's website[2] together with the results from simulations and other data for reacting plumes.

Yep *et al*. [33] and Pasumarthi & Agrawal [34] performed helium plume experiments in reduced gravity, using a drop tower facility at NASA. They showed that a naturally steady helium plume was up to 70% wider in microgravity than in normal earth gravity [33]. A plume at higher *Re* and *Ri* that exhibited puffing behaviour in earth gravity was found to produce steady flow behaviour in microgravity. This was taken as providing direct physical evidence that the oscillatory behaviour of low-density plumes is buoyancy induced.

Subbarao & Cantwell [22] investigated buoyant plumes of helium with a co-flow of air at a fixed velocity ratio of two. They examined the effects of varying the Richardson and Reynolds numbers independently within the range $390 < Re < 772$ and $0.58 < Ri < 4.97$, and examined the natural frequency of the oscillations and the transition to turbulence. Based on their findings, they proposed a buoyancy Strouhal number of the form:

$$St = \frac{\left(f\, D / V_0\right) - K_1}{Ri^{1/2}} \tag{11}$$

where K_1 is a constant, chosen as 0.445, and the density difference in the Richardson number is made dimensionless using the plume source density. In the range of flows they considered where $Ri > 1$, the buoyancy Strouhal number was found to be approximately constant at a value of 0.136.

Gebhart *et al*.'s works [19][35][36] have examined in detail the transition mechanisms and instability of laminar plumes, largely based on theoretical stability analysis and empirical studies. Some very early numerical simulations of plumes were performed in [35] where inviscid solutions of the Orr-Somerfield equations were obtained for symmetric and asymmetric plume disturbances.

O'Hern *et al*. [4][37] performed detailed experiments on turbulent helium plumes to help provide data for validation of LES models. Their facility at Sandia National Laboratories involved a main chamber with dimensions 6.1 × 6.1 × 7.3 metres and a 1 metre diameter plume source. The Reynolds number based on the inlet diameter and velocity was 3200 the Richardson number around 76. Measurements taken using Particle Image Velocimetry (PIV) and Planar Laser-Induced Fluorescence (PLIF) produced simultaneous time-resolved velocity and mass fraction data. This was used to calculate density-weighted Favre-averaged and Reynolds-averaged statistics. The detailed measurements were analysed to understand the dynamics of the unsteady plume and the role of the Rayleigh-Taylor instability in producing bubble and spike flow structures. The experiments were subsequently used in computational studies by DesJardin *et al*. [1], Tieszen *et al*. [2], Xin [3], Nicolette *et al*. [38], Chung & Devaud [39], Blanquart & Pitch [40] and Burton [41].

2 http://www2.bfrl.nist.gov/userpages/wmell/plumes.html

Computational Fluid Dynamics

CFD simulations of the unsteady near-field behaviour of buoyant plumes have mainly used Large-Eddy Simulation (LES) or Direct Numerical Simulation (DNS) rather than traditional Reynolds-Averaged Navier-Stokes (RANS) turbulence models.

There are two notable exceptions. Firstly, the work of Nicolette *et al*. [38], who performed RANS simulations using a newly-developed buoyancy-modified $k - \varepsilon$ model. The cases examined involved large-diameter helium plumes, including those studied experimentally by O'Hern *et al*. [4]. The axial velocity was overpredicted in the near-field due to delayed onset of transition to turbulence in the model. Results were also found to be sensitive to the grid resolution, with steady solutions at low resolution and unsteady solutions at high resolutions, using grids with more than 1 million cells. Their modified $k - \varepsilon$ model was found to be more numerically stable and gave better predictions over a broader range of grid resolution than the standard $k - \varepsilon$ model. The same research group also investigated a Temporally-Filtered Navier Stokes (TFNS) approach for modelling helium plumes [42].

The second notable RANS study is the recent work of Chung & Devaud [39], who used both buoyancy-modifed steady $k - \varepsilon$ RANS models and LES to study the large helium plumes examined experimentally by O'Hern *et al*. [4]. The RANS simulations were performed using the commercial CFD code, CFX, and the LES simulations using the Fire Dynamics Simulator (FDS) code from NIST[3]. For the RANS simulations, the flow was treated as axisymmetric and details of the experimental geometry, including the location of the co-flow air inlets and the ground plane were included in the model. Both Simple Gradient Diffusion Hypothesis (SGDH) and Generalized Gradient Diffusion Hypothesis (GGDH) models were tested and the sensitivity of the results to the modelling constant $C_{\varepsilon 3}$ was assessed[4]. For the LES, a simpler geometry was modelled with only the plume source and ground plane, and the sensitivity of the results to the Smagorinsky constant and the grid size was examined. Four different uniform Cartesian grids were tested for the LES with cell sizes ranging from 1/10 to 1/80 of the plume source diameter, producing grids with between 63,000 and 33 million cells. The RANS results showed very significant sensitivity to the choice of $C_{\varepsilon 3}$, with centreline velocities at a distance 0.4 diameters downstream from the source ranging from 0.85 to 5.0 m/s for values of $C_{\varepsilon 3}$ from 1.0 to 0.0, respectively, for the SGDH model. The GGDH was found to be even more sensitive to the choice of $C_{\varepsilon 3}$. This significant sensitivity to the choice of $C_{\varepsilon 3}$ compared to previous studies of the model behaviour in the far-field of buoyant plumes was attributed to the very large density difference in the near-field. Good predictions were obtained using $C_{\varepsilon 3} = 0.30$ for the SGDH model and $C_{\varepsilon 3} = 0.23$ for the GGDH model. The SGDH model gave best agreement with the experiments in terms of the mean concentrations, whilst the GGDH model gave overall slightly better agreement in terms of the streamwise velocity. It was noted by Chung & Devaud [39] that the $C_{\varepsilon 3}$ constant may need to be tuned to the particular buoyant plume conditions to obtain the best results. The LES predictions were in good agreement with the experimental measurements both in terms of the puffing frequency and the mean velocity, which was predicted to within the limits of experimental uncertainty up to an axial distance of 0.6 diameters downstream from the plume source. For the mean concentration, the peak centreline values were in good agreement with the measurements at the base of the plume but became overpredicted beyond a distance of 0.2 source diameters, and by 0.6 diameters the peak was more than a factor of two higher than the experimental values. The overprediction of concentration and, to a lesser extent, velocity, on the plume centreline was attributed to under-resolution of buoyancy-induced turbulence, which Chung & Devaud [39] suggested could be improved by using a more

3 For details of how to download the FDS code and relevant documentation, see http://www.fire.nist.gov/fds.

4 For more information on these model details, see the companion UFR on the far-field behaviour of plumes.

sophisticated subgrid-scale model that took into account the effects of backscatter. Best agreement with the experiments was obtained with the finest grid, although results with a grid of 4 million cells (a cell size of 1/40 of the source diameter) were nearly as good, and Chung & Devaud [39] considered them to provide an appropriate balance of accuracy and computational cost. Changing the Smagorinsky constant to values of 0.0, 0.1, 0.2 and 0.3 was found to affect mean velocity and concentration statistics differently at different positions. At an axial distance of 0.4 diameters, a value of C_s = 0.0 provided best agreement with the experiments whilst closer to the source a value of C_s = 0.1 produced better predictions. Overall, it was recommended to use values of C_s between 0.15 and 0.20 with a grid resolution of 4 million cells.

Amongst the earliest DNS studies of plumes are those published in 2000 by Jiang & Luo [20][21]. They examined both plane and axisymmetric non-reacting and reacting plumes with temperature ratios $\left(T_0/T_\infty\right)$ of 2, 3 and 6, and Reynolds number of 1000. The flows were treated as two-dimensional or axisymmetric. This choice was justified on the basis that previous fire-plume studies [43][44] had indicated that buoyancy-induced vortical structures were produced primarily by axisymmetric instability waves and therefore azimuthal wave modes could be ignored. The more recent study of DesJardin *et al*. [1] has highlighted that azimuthal instabilities are significant near the base of large helium plumes. Two-dimensional/axisymmetric simulations also do not capture the turbulent three-dimensional vortex stretching mechanism.

Jiang & Luo [20][21] used their DNS results to examine the budget of the vorticity transport equation. The production of vorticity near the base of the plume was found to be dominated by the gravitational torque in the initial phase of the vortex formation. Later, when the vortex had become more established and was convecting downstream, the baroclinic torque was found to be the dominant term. The gravitational torque was mainly responsible for the necking phenomenon near the base of the plume whilst the baroclinic torque was more important in forming necking and diverging sections of the vortical structures further downstream.

More recently, Soteriou *et al*. [24] performed high-resolution two-dimensional simulations of transitional plumes using a Lagrangian Transport Element Method. Simulations were compared to the planar helium plume experiments of Cetegen *et al*. [23]. The aim of their study was to understand the mechanisms involved in the near-field flow instability. The effects of changing the density ratio, the Reynolds number and Froude number (*S*, *Re* and *Fr*) were explored. The simulations captured the plume pulsation frequency and the correct overall instantaneous flow behaviour. The pulsation frequency was found to be insensitive to the Reynolds number, which confirmed previous observations from plume experiments [18][26]. Whilst experiments had suggested that the pulsation instability does not occur for plumes with density ratios less than $S \approx 1.7$ [18][27], the simulations by Soteriou *et al*. [24] found that pulsations were produced at lower values of *S*, but that the Froude and Reynolds numbers at which these pulsations were observed could not be easily achieved experimentally. It was also shown that a necessary condition for stable, steady plumes was for the circulation[5] to increase monotonically with height. This leads the flow induced into the plume to be directed inwards towards the plume axis (necking). A non-monotonic increase in the circulation (i.e. a local maximum) leads to vortex formation. Depending upon the relative magnitude of the local convective, buoyant and viscous forces, it was noted that a local circulation maxima could be smoothed out or amplified.

In the mid-1990's, Mell *et al*. [31][32] studied the behaviour of helium plumes using the FDS code. Axisymmetric simulations were compared to experiments undertaken in-house at NIST for Froude

5 The circulation, Γ, is defined as the integral of vorticity over a surface, $\Gamma = \int_S \omega \cdot dS$

numbers of $0.0015 \leq Fr \leq 0.64$ and Reynolds numbers based on the exit velocity and nozzle diameter of $22 \leq Re \leq 446$ (for details, see Mell's website[6]). Results from the simulations were in reasonable agreement with the experiments in terms of flow structures, puffing frequency, mean axial velocity and mean helium concentrations near the nozzle. At distances of more than 3 nozzle diameters downstream from the source, the agreement between simulations and experiments worsened – the axial mean velocity becoming overpredicted by nearly 40%. This was attributed to the increasing importance of three-dimensional turbulent flow structures with downstream distance which were not captured in their axisymmetric simulations. Mell *et al*. [31][32] also investigated the effect of neglecting the baroclinic torque term on the flow simulations. Neglecting the term was found to cause the plume to pulsate at significantly higher frequencies. More recent simulations by Xin [3], also undertaken using FDS, studied the helium plume experiments of O'Hern et al. [37] and investigated the influence of the baroclinic torque.

The works of Zhou *et al*. [45][46] were the first to examine the unsteady motion of plumes using LES all the way from the source to the fully-developed plume region in the far field where the flow exhibits self-similar behaviour. In their simulations, the flow domain extended to a distance of 16 nozzle diameters from the source. Their simulations were compared to the thermal plumes of George *et al*. [47] and Shabbir & George [48] ($Re = 1273$, $Fr = 1.4$) in [45] and to those of Cetegen [28] ($Re = 730$ and 1096, $Ri = 0.324$ and 0.432) in [46]. In both cases, the simulations used a low-Mach-number approach and a Smagorinsky LES model with constant coefficients ($C_s = 0.1$ and $Pr_t = 0.3$). The same grid of $256 \times 128 \times 128 \approx 4.2$M nodes for the domain of $16 \times 8 \times 8$ diameters was used in both cases. Good agreement was obtained between the LES results and the experiments in terms of the radial profiles of mean velocity and temperature in the self-similar plume region. The decay of mean centreline velocity and temperatures in the simulations followed the -1/3 and -5/3 decay laws characteristic of fully-developed plume behaviour. In the near-field of the plume, the dynamic puffing behaviour was reasonably well-captured when compared to the Cetegen & Kasper [18] correlation (Equation 6). In [46], the LES data was used to present budgets for various terms in the mean axial velocity, temperature, turbulent kinetic energy and temperature-variance equations in the fully-developed plume region. A more recent study by Zhou & Hitt [49] analysed the data obtained in one of their earlier studies using proper orthogonal decomposition.

A more recent study by Pham *et al*. [50] also simulated the full extent of a plume, from the source to the far field (up to an axial distance of $x/D = 80$) using DNS and LES. No inlet velocity was prescribed and instead the plume was produced by a circular flat plate heated to 673K, which gave Reynolds and Froude numbers of 7,700 and 1.1, respectively. The DNS grid comprised 660 million nodes, whilst two different LES grids were tested with 1.2 and 2.9 million nodes. The performance of several different subgrid-scale models were assessed including a Smagorinsky model (SM) with coefficients calibrated from the DNS, a dynamic model in which both the Smagorinsky constant and the turbulent Prandtl number were estimated using the dynamic procedure (DM), the Lagrangian dynamic model proposed by Meneveau *et al*. [51] combined with the dynamic model for the Prandtl number (LDM), and a modified Lagrangian dynamic model which used the Meneveau *et al*. [51] model for both Smagorinsky constant and Prandtl number (LDMT). The decay of mean velocity and temperature in the DNS were found to follow the -1/3 and -5/3 power law in the fully-developed plume region on the centreline. At an axial distance of 60 source diameters, the power spectrum of temperature fluctuations exhibited a -5/3 Kolmogorov power law decay on the axis, and a more rapid -3 power law decay at a lateral distance of 5 jet diameters, due to enhanced turbulence dissipation driven by buoyancy forces. The DNS solution was filtered using similar filter widths to those used by the LES and used to examine the budgets for the turbulent kinetic energy and heat flux transport equations. The mean values of the Smagorinsky constant and

6 http://www2.bfrl.nist.gov/userpages/wmell/plumes.html

turbulent Prandtl numbers were also extracted along the axis of the plume. Of the four models tested, the LDM and LDMT models were found to produce best agreement with the DNS in the far-field, in terms of both mean and fluctuating quantities. In the near field ($x/D < 4$), none of the models captured fully the correct behaviour, with all of the models under-predicting the plume width by around 20% and the SM and DM models over-predicting the peak velocity by 15% to 20%. Better predictions of the plume mean velocity and temperature were obtained with the LDM and LDMT models. Turbulence intensities were underpredicted by all models in the near field, by as much a factor of two in some cases for $x/D < 4$, although good agreement was obtained further downstream for $x/D > 4$. Overall, it was concluded that the LDMT model provided the best predictions of the purely thermal plume but that particular attention needed to be paid to the grid resolution near the plume source to capture the puffing phenomenon.

Worthy & Rubini [52][53][54] used LES to study the buoyant plumes of Shabbir & George [48] but only extended their flow domain to $x/D = 14$. They did not present comparisons between the results from their simulations and any experiments or empirical correlations. Instead, they focussed on the differences between various different LES subgrid-scale closure models, including variants of the standard Smagorinsky model, the dynamic Smagorinsky, the structure-function model of Metais & Lesieur [55], the one-equation model of Schumann [56] and mixed models based on the Leonard [57] and Bardina [58] approaches. Different scalar flux models based on the simple gradient diffusion and generalized gradient diffusion hypotheses (SGDH and GGDH) were also tested. They found significant differences between the results obtained using the different models. Purely dissipative SGS models were found to delay the onset of transition compared to mixed models. The grid they used was relatively coarse, composed of $127 \times 63 \times 63 \approx 0.5$M nodes for the domain size of $14 \times 7 \times 7$ diameters. Compared to the earlier simulations of Zhou *et al*. [45][46], cells were nearly double the size in each direction. It was also found necessary to use upwind-biased third-order and second-order convection schemes in the momentum and energy equations to obtain a stable solution, whereas Zhou *et al*. [45][46] were previously able to use central differencing schemes.

DesJardin *et al*. [1] performed large-eddy simulations of the helium plume experiments O'Hern *et al*. [4] with a fully-compressible code using two different grid resolutions, 512K and 2.5M cells. Results were presented both with without a SGS model. At the base of the plume, the LES was found to overpredict the RMS streamwise velocity and concentration. This was attributed to poor resolution of buoyancy-induced vorticity generation. Tieszen *et al*. [2] also examined the O'Hern *et al*. [4] helium plumes using an energy-preserving low-Mach-number code, combined with a dynamic Smagorinsky LES model and grids with 250K, 1M and 4M cells. Results were found to improve with grid resolution and it was postulated that this was related to the strong influence on the mean flow behaviour of small-scale Rayleigh-Taylor structures at the base of the plume. The works of DesJardin *et al*. [1] and Tieszen *et al*. [2] are discussed in more detail below.

A later study by the same group [40] examined the O'Hern *et al*. [4] helium plumes using the Lagrangian dynamic SGS model of Meneveau *et al*. [51] for turbulent diffusion terms in both the momentum and helium mass-fraction transport equations (modelled in their case as a mixture fraction). The full three-dimensional geometry of the experiments was simulated, including the plume source, ground plane and air co-flow injection flows, using a non-uniform cylindrical mesh with $192 \times 187 \times 64 \approx 2.3$M cells. The helium inlet velocity was lowered from the experimental Reynolds-averged value of 0.325 m/s to 0.299 m/s to account for the open area of the honeycomb (92%). The predictions of the mean and RMS velocity, and mean helium mass fraction were in good agreement with the experiments, in most cases within the limits of experimental uncertainty, and better than the earlier simulations of DesJardin *et al*. [1]. Close to the base of the plume (within

0.1 diameters) the centreline mean helium mass fraction was underpredicted and the RMS mass fraction was overpredicted, by up to a factor of two. These differences did not appear to have a significant effect on the flow downstream and it was noted that results may be improved by modelling more accurately the helium flow through the honeycomb immediately upstream of the plume source. Further downstream from the source, RMS mass fractions tended to be overpredicted and it was noted that an improved SGS model may be needed that takes account of buoyancy-induced turbulence.

A recent study by Burton [41] used a more advanced non-linear LES (nLES) subgrid-scale model to study the O'Hern *et al*. [4] helium plumes. Unlike the Smagorinsky class of models, the nLES model does not involve any artificial viscosities or diffusivities and instead models the unknown non-linear term in the filtered Navier-Stokes equations directly [59][60]. A uniform cylindrical grid was used with $128 \times 64 \times 32 \approx 0.3$M cells for a flow domain which extended four metres in diameter and ten metres in the axial direction. Using 64 cells across the diameter of the domain, the width of each cell was 1/16 of the plume source diameter, or five times the width of the cells in the finest LES grid used by Chung & Devaud [39]. Despite this relatively coarse grid, the difference in the plume puffing frequency between the model and the experiments was less than 8% and the mean and RMS velocity and concentration profiles were largely within the limits of the experimental uncertainty. Although the results presented by Burton [41] are therefore among the best of the LES model results published to date, radial profiles were not presented at all of the measurement locations, the centreline velocity at a position 0.1 diameters from the source appeared to be overpredicted by around 20% and issues such as grid-dependency were not discussed. Nevertheless, the encouraging results show some promise of what may be achieved with more advanced turbulence closures.

Other related CFD simulations of unsteady plumes include the works of Wen, Kang and colleagues at Kingston University who have studied the transient near-field behaviour of fire plumes [61][62], and Baastians *et al*. [63] at the J.M. Burgers Centre for Fluid Dynamics in Delft who have performed DNS and LES of plumes in a confined enclosure.

2.2.1 Studies on which this UFR review will be based

This UFR focuses on three separate studies which have each examined the detailed 1-metre-diameter helium plume experiments of O'Hern *et al*. [4]:

- **DesJardin *et al***. [1] (2004): simulations using a fully-compressible code with high-order upwind-biased convection schemes and a dynamic Smagorinsky model with grids of 512K and 2.5M cells.
- **Tieszen *et al.*** [2] (2004): simulations using an energy-preserving low-Mach-number code, combined with a dynamic Smagorinsky LES model and using grids with 250K, 1M and 4M cells.
- **Xin** [3] (2005): simulations using the Fire Dynamics Simulator (FDS) code from NIST, a low-Mach-number LES code using a Smagorinsky model with fixed coefficients and a grid of 1.5M cells.

Different numerical methods, grid resolutions and turbulence models are used in these three studies, and they therefore provide useful complementary data on the performance of CFD models which provides a good match for what is required in this UFR. Additional comments on model

performance are also provided in the works of Chung & Devaud [39], Blanquart & Pitch [40] and Burton [41], who also simulated the helium plume experiments of O'Hern *et al*. [4]. These recent works were published after this UFR was first completed, in 2007, and so are not examined in such detail here.

3 Test Case

3.1 Brief Description of the Study Test Case

- A summary of the boundary conditions is shown in Figure 8.
- A gas mixture mainly composed of helium is discharged through a circular orifice into ambient air.
- The gas is composed of 96.4% helium, 1.7% acetone and 1.9% oxygen by volume.
- The molecular weight of the gas released is 5.45 g/mol ± 2.7%.
- The mixture is discharged at a temperature of T_{He} = 11°C ± 3°C and the air is at T_{air} = 13 °C ± 3°C.
- The circular plume source has diameter, D = 1 metre.
- The helium is discharged at a Reynolds-averaged velocity V_0 = 0.325 m/s ± 1.3% and a Favre-averaged velocity of approximately 0.339 m/s.
- The flow through the orifice is laminar.
- The ambient pressure is 80.9 kPa ± 0.4 kPa.
- The measurements include:
    1. Time-history of vertical velocity at a point 0.5 m from the centreline and 0.5 m above the inlet, used to estimate the puffing frequency
    2. Measurements on a vertical plane through the plume from the plume source to a distance of one orifice diameter of:.
        a) Reynolds-averaged and Favre-averaged mean axial and radial velocities
        b) Reynolds-averaged and Favre-averaged shear stresses, normal stresses and turbulent kinetic energy[7]
        c) Favre-averaged helium concentrations
    3. Movies of helium concentration and velocities
    4. Profiles of the mean and RMS velocities, and mean and RMS helium concentrations at six measurement positions (0.1, 0.2, 0.3, 0.4, 0.5 and 0.6 m downstream of the plume source)

  Item 1 is available in the O'Hern *et al*. [4] paper, Items 2 and 3 can be obtained by contacting the authors of the study[8] and Item 4 is presented by Chung & Devaud [39].

7 Only velocities parallel to a two-dimensional plane were recorded. The turbulent kinetic energy, k, is calculated from the vertical and horizontal normal stresses ($\overline{uu}$ and $\overline{ww}$) by assuming that the horizontal component is the same in the out-of-plane direction ($\overline{vv}=\overline{ww}$), i.e. assuming that $k \approx (\overline{uu}+2\,\overline{ww})/2$.

8 Dr. Tieszen (srtiesz@sandia.gov) or Dr. O'Hern (tjohern@sandia.gov).

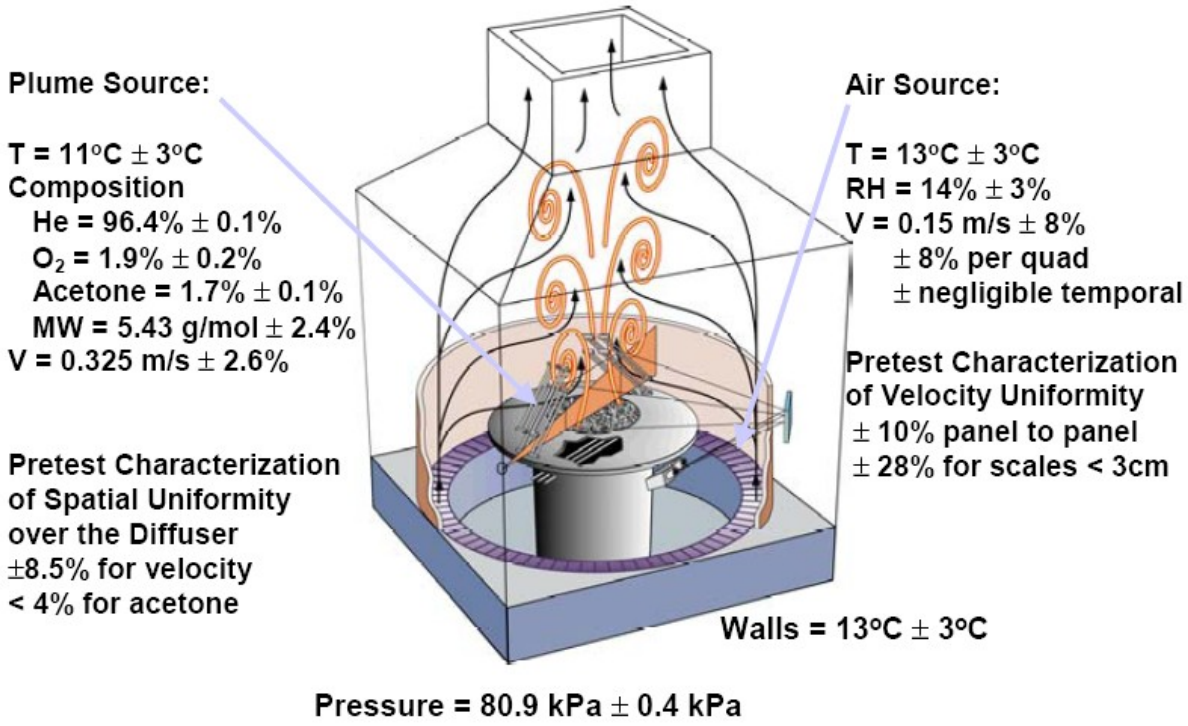

Figure 8 Boundary conditions for the O'Hern *et al*. [4] experiments

3.2 Test Case Experiments

The experiments selected for this UFR are those undertaken by O'Hern *et al*. [4] at the Fire Laboratory for Accreditation of Models by Experimentation (FLAME) facility at Sandia National Laboratories, Albuquerque, New Mexico, in the late 1990's/early 2000's. The aim of these experiments was to examine the characteristics of turbulent buoyant plumes and provide data that could be used to help validate LES models suitable for modelling fires.

The experimental arrangement is shown in Figures 8 and 9. The main chamber has dimensions 6.1 × 6.1 × 7.3 metres and converges to a square chimney outlet at the top with nominal dimensions of 2.4 m on each side. The plume source is located in the centre of the chamber 2.45 m off the floor. Air is directed through a series of diverters, screens and honeycombs to form an annular low-velocity inlet flow surrounding the helium plume. A relatively large plume source (diameter, D = 1 m) was chosen to ensure that the plume would be fully turbulent. This is surrounded by a 0.51 m wide sheet of steel which simulates the ground plane. Air is drawn into the helium plume passing over this sheet flowing radially inwards. The experiments were designed specifically to mimic an unconfined plume on an infinite ground plane with negligible wind effects. Extensive CFD simulations were performed to help design the facility and to ensure that any separation bubble formed by the vertical flow of air around the 0.51 m ground plane did not disturb the plume[9].

The helium flowed through a diffuser, a series of perforated plates and three layers of honeycomb before being released through the orifice. The honeycomb immediately upstream of the orifice suppressed turbulence and flow visualization suggested that the inflow conditions were laminar. A detailed study of the inlet flow characteristics also found that the inlet velocity profile was uniform

9 S. Tieszen, Private Communication, March 2010.

to within 6% [64]. Within just a few centimetres downstream of the inlet, observations suggested that the plume had become fully-turbulent. To ensure that the flow had reached a quasi-steady state, the helium was released for a couple of minutes before recordings were taken. Particle Image Velocimetry (PIV) was conducted using around 11,500 images spanning 70 puff cycles while Planar Laser-Induced Fluorescence (PLIF) analyses were performed on approximately 2,300 images, covering 33 puffs. The experiments were repeated 10 times and the inlet velocity was on average 0.325 m/s ± 1.3% [4]. The acetone and oxygen needed to be added into the helium released in order for laser fluorescence. As a consequence, the molecular weight of the mixture was 5.45 g/mol ± 2.7% compared to the pure helium value of 4.00 g/mol.

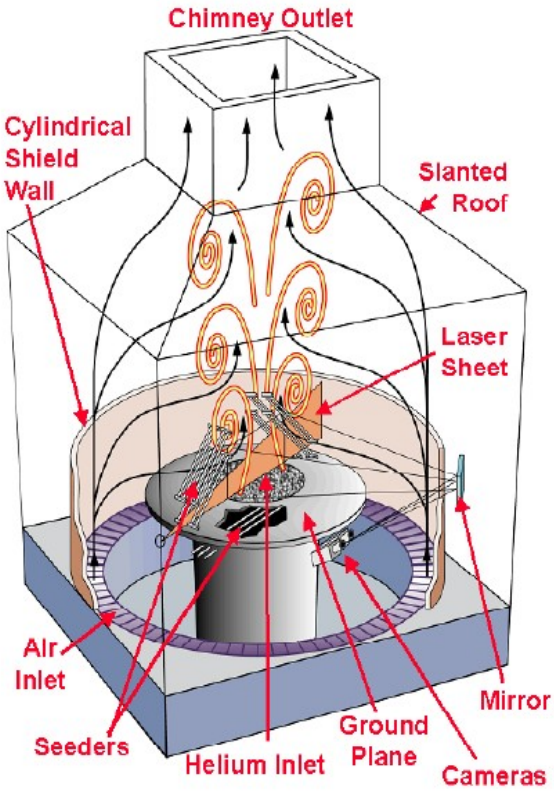

Figure 9 Schematic of the Sandia FLAME facility showing the laser-light sheet that bisects the plume and two video cameras that record the PIV and PLIF images.

The Reynolds number based on the inlet diameter and velocity, and the helium mixture properties was $Re = DV_0/\nu = 3200 \pm 0.6\%$ and the Richardson number was $Ri = (\rho_\infty - \rho_0)\, g\, D / (\rho_\infty V_0^2) = 76 \pm 6.5\%$, where ρ_∞ is the air density and ρ_0 the plume fluid density.

The PIV and PLIF measurements produced simultaneous time-resolved velocity and mass fraction data. The data was used to calculate density-weighted Favre-averaged statistics in addition to the more usual Reynolds or time-averaged statistics. Interestingly, the difference between the Favre- and Reynolds-averaged quantities was found to be less than the uncertainty in the data throughout the flow field [4].

The puffing frequency of the plume was analysed from the time-history of the vertical velocity at a

point in space 0.5 m above the inlet and 0.5 m radially from the centreline. The recorded mean measured frequency was 1.37 Hz which compares well with the empirical correlation of $f = 0.8\, V_0\, Ri^{0.38} / D$ from Cetegen & Kaspar [18] for helium-air plumes with $Ri < 100$, which gives a frequency of 1.35 Hz, and the empirical correlation of $f = 1.5\, D^{-1/2}$ from Cetegen & Ahmed [25] for fire plumes which gives a frequency of 1.5 Hz.

O'Hern *et al.* [4] discussed in some detail the dynamics of the unsteady plume and the role of the Rayleigh-Taylor instability in producing bubble and spike flow structures. Figure 10, taken from their paper, shows four snapshots of the plume where the spike and bubble structures are identified with arrows and the location of the large coherent puffing vortex is indicated with a circle.

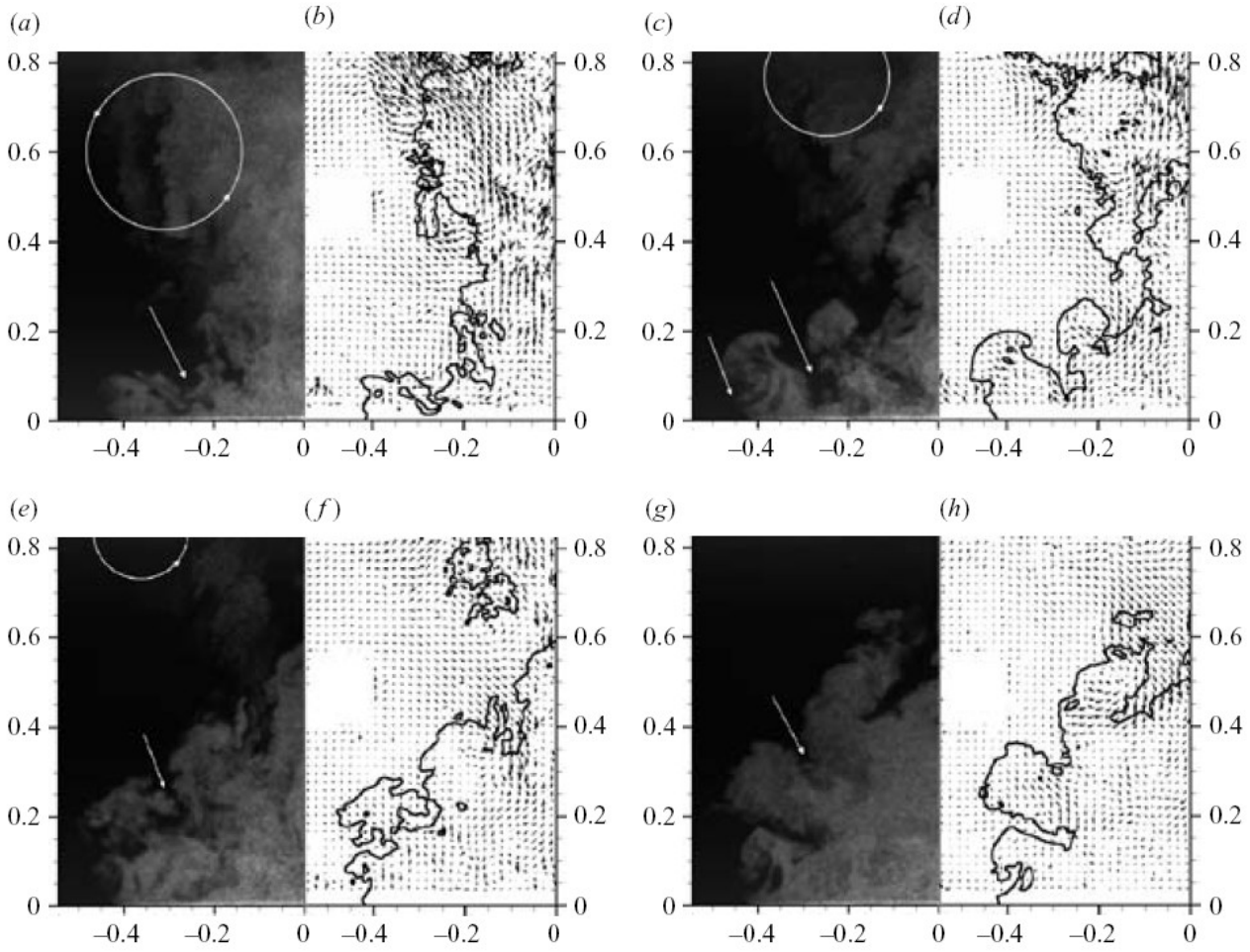

Figure 10 Four snapshots of the helium plume of O'Hern *et al*. [4] taken 115 ms apart. The left-hand-side of each image shows the mass fraction field from the PLIF, the right-hand-side shows the corresponding PIV vector field overlaid with the general plume outline. The development and movement of a large toroidal vortex is indicated by circular arrows. The spike and bubble structures characteristic of Rayleigh-Taylor instability are indicated by straight arrows.

Details of the uncertainties in the experiments are discussed at length in their paper. These include measurement errors due to the effects of out-of-plane motion and improper choice of peak correlation in the cross-correlation analysis of the PIV measurements, and the influence of film response, image registration and laser-sheet intensity normalization in the PLIF measurements.

Overall, the uncertainties are estimated to be ± 18% for the difference between the plume and air density, ± 5% for the air density, ± 20% for the velocities and ± 30% for the turbulence statistics [2].

3.3 CFD Methods

3.4 DesJardin et al. [1]: Description of CFD Work

3.4.1 Governing Equations

DesJardin *et al*. [1] used the fully-compressible form of the Favre-averaged Navier-Stokes equations. Transport equations were solved for the Favre-averaged momentum, species mass fraction and energy:

$$\frac{\partial(\rho U_i)}{\partial t}+\frac{\partial(\rho U_i U_j+p\,\delta_{ij})}{\partial x_j}=\frac{\partial}{\partial x_j}\left[\mu\left(\frac{\partial U_i}{\partial x_j}+\frac{\partial U_j}{\partial x_i}\right)-\frac{2}{3}\mu\frac{\partial U_k}{\partial x_k}\delta_{ij}\right]+\frac{\partial \tau_{u_i u_j}}{\partial x_j}+\rho g_i \tag{12}$$

$$\frac{\partial(\rho Y)}{\partial t}+\frac{\partial(\rho U_j Y)}{\partial x_j}=\frac{\partial}{\partial x_j}\left(\frac{\mu}{Sc}\frac{\partial Y}{\partial x_j}\right)+\frac{\partial \tau_{u_j Y}}{\partial x_j} \tag{13}$$

$$\frac{\partial(\rho e)}{\partial t}+\frac{\partial(\rho U_j h)}{\partial x_j}=\frac{\partial}{\partial x_j}\left[\frac{\mu c_p}{Pr}\left(1-\frac{Pr}{Sc}\right)\frac{\partial T}{\partial x_j}+\frac{\mu}{Sc}\frac{\partial h}{\partial x_j}\right]+\frac{\partial \tau_{u_j h}}{\partial x_j}+\frac{\partial \tau_{u_j u_k u_k}}{\partial x_j}+\frac{\partial\left(U_k \tau_{u_j u_k}\right)}{\partial x_j}+\rho U_k g_k \tag{14}$$

where ρ is the density, U_i the velocity components, p the pressure, Y the species mass fraction, e the total energy and h the enthalpy (*N.B.* all of these parameters are Favre-averaged quantities). For the diffusion of helium into air, the molecular Schmidt and Prandtl numbers were set to values of Sc = 0.2 and Pr = 0.7. Thermodynamic properties, such as c_p, were evaluated based on the mixture composition using the Chemkin libraries. The molecular viscosity, μ, was determined from Sutherland's law for pure air.

3.4.2 Turbulence Modelling

The Smagorinsky model was used for the SGS stresses in the momentum equation, $\tau_{u_i u_j}$, and a simple Boussinesq gradient-diffusion model was used for the SGS stress terms in the species mass fraction and energy equations, $\tau_{u_j Y}$ and $\tau_{u_j h}$:

$$\tau_{u_i u_j}=2\rho C_R \Delta^2 |S|\left(S_{ij}-\frac{1}{3}S_{kk}\delta_{ij}\right) \tag{15}$$

$$\tau_{u_j Y}=2\rho C_Y \Delta^2 |S|\left(\frac{\partial Y}{\partial x_j}\right) \tag{16}$$

$$\tau_{u_j h}=2\rho C_h \Delta^2 |S|\left(\frac{\partial h}{\partial x_j}\right) \tag{17}$$

where $S_{ij}=1/2\left(\partial U_i/\partial x_j+\partial U_j/\partial x_i\right)$ is the strain rate and $|S|=\left(2S_{ij}S_{ij}\right)^{1/2}$ is the strain-invariant. The filter width was taken as twice the cube-root of the local computational cell volume, $\Delta=2(\delta x\,\delta y\,\delta z)^{1/3}$, where δx, δy, and δz, are the cell widths. This is twice as large as the commonly used value and was chosen in an effort to minimize numerical errors. The three modelling "constants", C_R, C_Y and C_h were calculated dynamically [65][66] using a second explicit filter that was twice the size of the first implicit filter. To ensure numerical stability, the constants were locally smoothed using explicit filtering with a filter function described by Fureby [67]. The

magnitude of the effective viscosity or diffusivity was also clipped to be always greater than or equal to zero ($\mu+\mu_t \geqslant 0$ and $D+D_t \geqslant 0$). DesJardin *et al*. [1] noted that the advantage of this approach over other approaches is that it allows for some backscatter that may be important for laminar to turbulent transition. Triple correlations appearing in the energy equation, $\tau_{u_j u_k u_k}$, were modelled using an approach proposed by Ragab *et al*. [68][69], for details see [1]. DesJardin *et al*. [1] also presented results obtained without using the SGS model (i.e. a "no-model" approach).

3.4.3 Numerical Methods

DesJardin *et al*. [1] used a finite-volume treatment where the mass, momentum and energy equations equations were differenced in time using a fourth-order Runge-Kutta scheme. Convective terms were discretized using a blend of a fifth-order ENO scheme for the first two stages of the Runge-Kutta integration and ninth-order upwind-biased scheme for the final two stages. This combination of high-order schemes was chosen to prevent dispersive errors (undershoots and overshoots), minimize numerical dissipation and avoid odd-even decoupling errors (chequerboarding) in regions of the flow where the Mach number was small. Where the flow was aligned to the grid, their approach should have provided up to ninth-order accuracy for the momentum equations and fifth-order accuracy for mass, energy and species mass fraction. Diffusion terms were discretized using fourth-order central differences. Near the boundaries, the differencing schemes used for the convection and diffusion terms were of lower order accuracy.

To avoid having to use a time-step limited by the acoustic wave speed, DesJardin *et al*. [1] used the Pressure Gradient Scaling (PGS) method of O'Rouke *et al.* [70][71]. This approach decomposes the pressure into two parts comprising thermodynamic and hydrostatic components. The thermodynamic component, which contains acoustic information, is pre-multiplied by a scaling factor which artificially reduces the acoustic wave speeds. Details of this technique are given in the Appendix of DesJardin *et al*.'s paper [1].

3.4.4 Boundary Conditions

The vertical boundaries and top outlet planes were assumed to be open, allowing for flow to be entrained into or exit the domain. On the inlet plane, the inlet velocity for the helium was U_p = 0.351 m/s, whereas the experimental Favre-averaged velocity was 0.339 m/s [4]. A small axial coflow velocity of 0.01 m/s was specified outside the plume whereas in the experiments there was a fixed ground plane. The cross-stream velocities were set to zero on the inlet plane. A considerable amount of detail on the treatment used to avoid acoustic waves reflecting back from open boundaries into the domain and contaminating the solution was provided in an Appendix to their paper [1]. The non-reflective pressure relation used at open boundaries was based on an approach developed by Rudy & Strikwerda [72][73]. In the simulations, the gas released was pure helium with a molecular weight of 4.0 g/mol, whilst in the experiments, the gas released had a molecular weight of 5.4 g/mol.

The inlet velocity, the co-flow and the gas density differed slightly compared to the experiments since the simulations and the experiments were undertaken concurrently, and the final measured conditions differed from those originally planned[10].

It was not found necessary to superimpose turbulent fluctuations on the inlet velocity to obtain transition to turbulence. Tests found that using different prescribed inlet turbulence intensities did not affect the resulting flow behaviour[11].

10 *DesJardin, Personal Communication, 2010.*
11 *DesJardin, Personal Communication, 2007.*

3.4.5 Grid Used

Rather than model the same geometry as used in the experiments, it was assumed that the experimental conditions represented an unconfined plume. The computational domain was then constructed as a cube with sides of length 4 metres. DesJardin *et al*. [1] commented that this domain size was found necessary for the plume to be unaffected by the presence of the domain boundaries, due to the large quantity of air drawn into the plume in each puffing cycle. Note that in comparison, the central chamber of the FLAME facility, where the experiments were conducted, comprised a cube of sides 6.1 m and the ground plane around the plume source extended 0.51 m radially outwards from the perimeter of the source orifice (see Figure 9). Two grids were used comprising 80 × 80 × 80 (= 512k nodes) and 136 × 136 × 136 (≈ 2.5M nodes). The grids were refined near the centreline and the base of the plume resulting in minimum and maximum grid spacings of 2.8 cm and 13.1 cm for the coarse grid and 1.6 cm and 7.8 cm for the fine grid. A plot showing a cross-section through the mesh is given in their paper. It is not clear how the circular inlet orifice was modelled using the structured mesh although from their plot of the grid it would appear that a stair-stepped or sawtoothed approach was probably taken.

3.4.6 Time-Averaging

Calculations were run for 10 seconds of physical time to allow for initial transients to move downstream and for the flow to develop. Another 10 seconds of physical time were then used to collect at least 2000 realizations of the flow field for constructing mean and RMS values.

Calculations were performed using 128 processors with typical run times of 5.5 hours/processor for a every second of physical time (a total CPU time of ~14,000 hours).

3.4.7 Discussion

The CFD methodology employed by DesJardin *et al*. [1] appears to have been performed to a high standard. Details of the modelling and numerical techniques used in their work were recorded clearly in their paper.

A number of studies have shown that upwind-biased numerical schemes should be avoided when using LES, since they can lead to excessive numerical dissipation [74][75]. DesJardin *et al*. [1] recognized that the use of upwind-biased convection schemes could introduce some undesirable numerical errors. They noted that whilst pure central-differencing schemes are commonly used in non-reacting flows, some degree of upwinding is necessary to stabilise the solution when there are strong scalar gradients. They chose a high-order upwind scheme to minimize unwanted dissipation and noted that they did not expect the flow predictions to be sensitive to the details of the discretization scheme.

The difference of more than 20% in the density of the gas released in their model compared to that released in the experiments is unfortunate and may have affected their results. Similarly, small errors may have been introduced by using a 0.01 m/s co-flow, and an inlet velocity of 0.351 m/s instead of the experimental Favre-averaged value of 0.339 m/s [4].

3.5 Tieszen et al. [2]: Description of CFD Work

3.5.1 Governing Equations

Tieszen *et al*. [2] used a low-Mach-number code developed at Stanford University by Pierce [76]

[77]. In the low-Mach-number limit, acoustic interactions, compressibility effects and viscous dissipation effects are neglected. The pressure is decomposed into a background pressure, p_0, and a flow-induced perturbation pressure, δp. The background component is assumed to be constant in space and time and is used in the energy equation and the state equation (the ideal gas law). For details of the equations solved, see [76].

3.5.2 Turbulence Modelling

The basic turbulence model used was the same as that employed by DesJardin *et al*. [1] (see above). This comprised the Smagorinsky LES model with coefficients determined using the dynamic procedure of Germano *et al*. [65] and the least-squares approach of Lilly [66]. Details of the averaging procedure used to smooth the dynamic constants are not provided in the paper by Tieszen *et al*. [2]. The test filter used in the dynamic procedure was twice the width of the grid filter. Subgrid-scale effects in the species mass fraction and energy equations were modelled using a gradient-diffusion approach.

3.5.3 Numerical Methods

The cylindrical form of the governing equations were solved and a structured mesh was used. Velocities were stored at staggered locations with respect to density and other scalars in both space and time. An energy-conservative, second-order central differencing scheme was used for convection in the momentum equations and an upwind-biased QUICK differencing scheme was used for the scalar equations. An iterative semi-implicit approach was used in time similar to the Crank-Nicolson scheme.

3.5.4 Boundary Conditions

For the boundary conditions, Tieszen *et al*. [2] stated simply that open boundaries were used on all domain surfaces except the floor and inlet. They noted that the inlet treatment differed slightly to that of DesJardin *et al*. [1] in that the flow in the diffuser is not specified directly using a Dirichlet condition but allowed to develop, ignoring the presence of the honeycomb at the inlet. Although this is not clear, it suggests that rather than impose a flat top-hat profile at the inlet, the flow was allowed to develop for some distance upstream of the orifice before discharging into the main flow domain.

3.5.5 Grid Used

Tieszen *et al*. [2] did not describe the overall size of the cylindrical domain used in their study, although from one of their figures (copied in Figure 14, below) it appears that it extended at least 1.6 metres radially and 2.7 metres axially. A structured mesh was used and grid-sensitivity studies were undertaken using three different mesh densities: a coarse mesh comprising in total around 250k nodes with 52 × 64 × 80 nodes in the radial × azimuthal × axial directions, a medium mesh of approximately 1M nodes (104 × 64 × 160), and a fine mesh with 4M nodes (208 × 64 × 320). In each case, the same number of nodes was used in the azimuthal direction. No details are given regarding any clustering of nodes and a plot of the mesh was not provided in their paper.

3.5.6 Time-Averaging

Time-averaging was performed once the flow had established a quasi-steady puffing mode. No further details were provided regarding the time-period over which averaging was performed.

3.5.7 Discussion

The description of their work in Tieszen *et al*.'s paper [2] was not comprehensive and some important details, such as the size of the flow domain, the smoothing of the dynamic Smagorinsky constant, the time-averaging and the nature of the boundary conditions were not provided. Since the principal author, Tieszen, was a co-author of both the computational work of DesJardin *et al*. [1] study and the experiments of O'Hern *et al*. [4], it is reasonable to assume that appropriate choices were made for these aspects of the modelling and that their description was omitted simply in order to keep the paper concise. Tieszen *et al*.'s study provides useful information on grid-dependence issues which are critical to understand for industrial LES. The main objective of the paper was to outline plans for a buoyancy-modified SGS model, which is discussed later.

3.6 Xin [3]: Description of CFD Work

3.6.1 Numerical Methods

Xin [3] used the open-source LES-based CFD code: Fire Dynamics Simulator (FDS) version 3 which is developed and maintained by the U.S. National Institute for Standards & Technology (NIST). The code solves the low-Mach-number equations on a staggered Cartesian grid. The spatial discretization is second-order accurate and an explicit second-order predictor-corrector method is used in time.

3.6.2 Turbulence Modelling

FDS uses the Smagorinsky SGS model with constants of C_s = 0.2, Pr = 0.7 and Sc = 1.0. The model in this version of FDS was implemented in a rather unusual way. The diffusion term in the momentum equation is usually written:

$$\frac{\partial}{\partial x_j}\left[\left(\mu+\mu_t\right)S_{ij}\right] \tag{18}$$

where μ is the molecular viscosity, μ_t is the SGS viscosity and S_{ij} is the strain-rate. In this version of FDS, the model was implemented as follows:

$$\frac{\partial}{\partial x_j}\left[max\left(\mu\,,\,\mu_t\right)S_{ij}\right] \tag{19}$$

i.e. the effective viscosity was taken as either the molecular viscosity or the SGS viscosity, whichever was largest.

3.6.3 Boundary Conditions

All of the boundaries were treated as openings except for the floor. At these openings the total specific pressure was set to zero if the flow was entering the domain or to $u^2/2$ if the flow was leaving (see [78] for details). Air entering the domain was assigned ambient conditions. For the plume source, Xin [3] used an inlet flow velocity of 0.351 m/s which was superimposed with 1% random noise. This is the same mean velocity as that used by DesJardin *et al*. [1], despite the the experimental Reynolds and Favre-averaged velocities being 0.325 m/s and 0.339 m/s [4].

3.6.4 Grid Used

A rectangular computational domain was used with dimensions 2 × 2 × 6 metres. This corresponds to half the width and one-and-a-half times the height of the domain used by DesJardin *et al*. [1]. Since FDS uses a Cartesian grid, the circular inlet was modelled as a stair-stepped or sawtoothed

shape. To help reduce unphysical vorticity being produced on surfaces with stepped boundaries, the 'sawtooth' model can be activated in FDS [78]. It is not clear from the description given in Xin's paper [3] whether or not this model was used.

The Cartesian grid was composed of grid with cells of sides 2.5 cm. This gives a mesh of 80 × 80 × 240 nodes with in total approximately 1.5M nodes.

3.6.5 Time-Averaging

Xin [3] stated that calculations were run for 20 seconds during which time there were more than 12 puffing cycles. During each simulation 1000 data samples were taken which were used for time-averaging. It is unclear from the description whether a period of time was allowed for the flow to develop before sampling took place.

3.6.6 Discussion

Details of the modelling and numerical techniques are only briefly described by Xin [3]. This reflects the fact that it was only a conference paper and not a peer-reviewed journal article.

The computational domain used was relatively small, only half the width of that used in the earlier study by DesJardin *et al*. [1]. In their paper, DesJardin *et al*. noted that a relatively large computational domain was necessary for the plume development to be free from the influences of the domain boundaries. It is possible therefore that some boundary effects could have influenced Xin's results. Given the strong dependence of LES flow predictions on the grid resolution, the choice of a small domain may have been driven by the desire to maximise the grid refinement at the possible expense of introducing some boundary effects.

There have been various different values proposed for C_s: for example, a value of 0.17 for homogeneous isotropic turbulence [56], 0.1 for mixing layers [79], and 0.065 for channel flows [80]. The constant has to be reduced to obtain the correct asymptotic flow behaviour near walls and the optimum value of C_s is also a function of the computational grid resolution [81]. It is reasonable to surmise that the Smagorinsky constant is not really a constant at all but a parameter dependent on the flow and the grid resolution. In Xin's simulations, the Smagorinsky constant was taken as the default FDS value of 0.2 throughout the whole flow domain. This may have lead to excessive damping of the turbulent structures in some regions of the flow. The sensitivity of LES predictions to the Smagorinsky constant was examined by Chung & Devaud [39], who also used the FDS code. They found that values of C_s between 0.15 and 0.20 produced the best overall agreement with the experiments of O'Hern *et al*. [4].

4 Evaluation

4.1 Comparison of DesJardin et al. [1] CFD Calculations with Experiments

Figure 11 shows a snapshot of the flow field predicted by the CFD model of DesJardin *et al*. [1]. With the coarse grid, the plume puffing frequency was found to be approximately 1.8 Hz, much higher than the frequency measured in the experiments of 1.37Hz. The predictions improved as the grid was refined, with the fine grid producing a frequency of 1.5 Hz. A similar frequency was obtained with or without an SGS model. DesJardin *et al*. [1] also presented results from a simulation with no SGS model and a very coarse mesh (220k nodes in total and only 30 cells across the source diameter). This produced a puffing frequency of 1.7 Hz, which they considered to be an adequate estimate for engineering purposes, although the axial velocity in this case was overpredicted by nearly a factor of two.

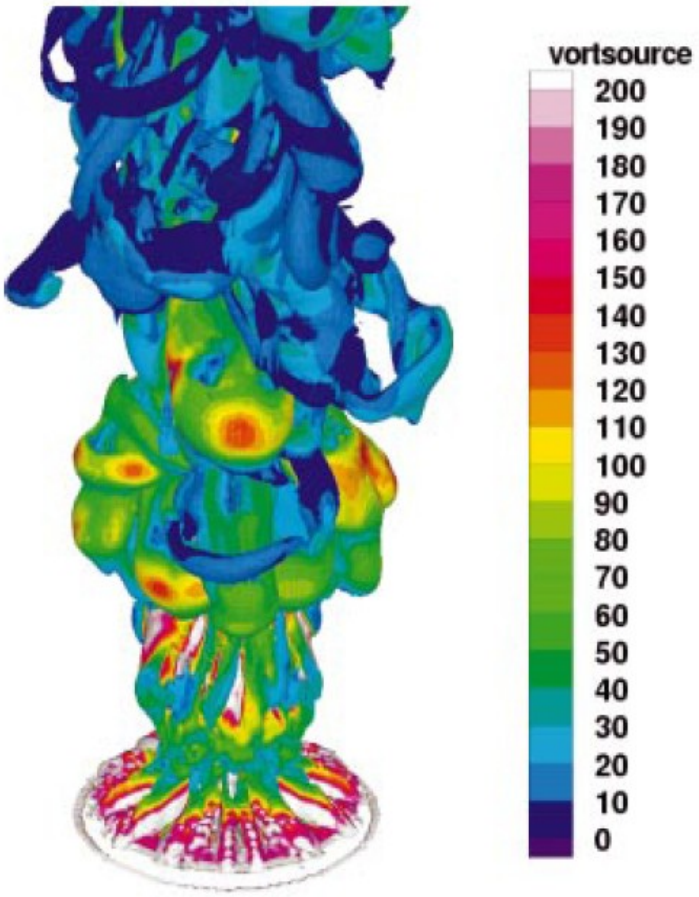

Figure 11 An instantaneous snapshot of the DesJardin *et al*.'s LES predictions showing an iso-contour of vorticity magnitude at 5% of the maximum coloured according to the magnitude of the gravitational torque.

Figure 12 shows the mean axial velocity predictions at three vertical positions within the plume. The symbols are the experimental data points with their uncertainty shown as vertical lines. The

predictions are overall in good agreement with the experiments. All of the results are mostly within the experimental uncertainty bounds except for the results obtained using the coarse 512k node mesh with an SGS model. For this case, the peak velocity is overpredicted by 27 %, 61 % and 67 % at the three downstream positions x = 0.2 m, 0.4 m and 0.6 m. For the coarse mesh, mean axial velocity predictions are improved when the SGS model is not used. DesJardin *et al*. suggested that the relatively poor predictions with the coarse grid and SGS model were due to there being a net upscale transport of turbulent energy near the plume source, from small to large scales. They noted that the purely dissipative Smagorinsky model was unable to account for this phenomenon. Using finer meshes, a greater proportion of turbulence energy was resolved. Alternatively, by removing the SGS model, the damping from the turbulence model was reduced, which improved the predictions.

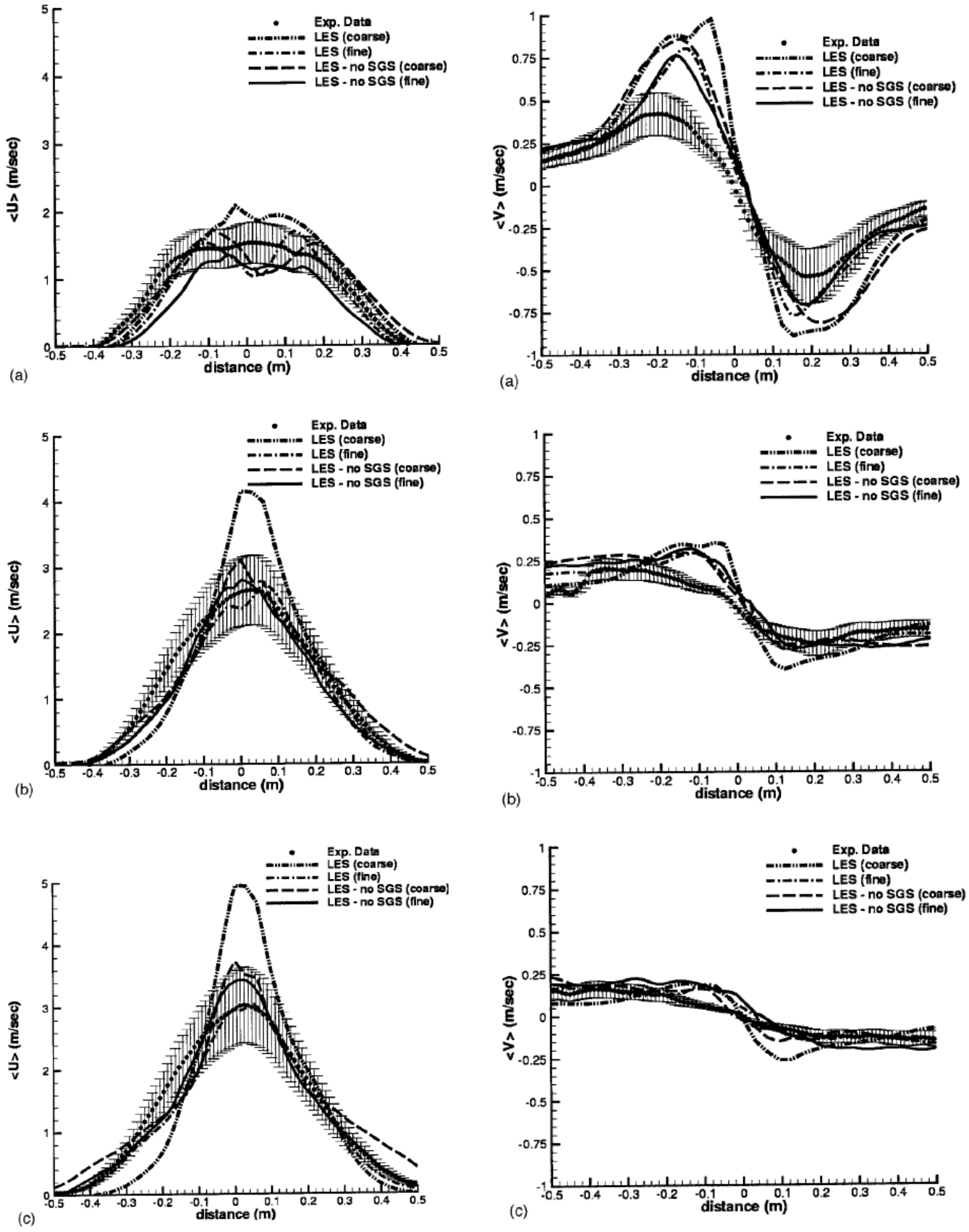

Figure 12 Mean axial velocity (left) and radial velocity (right) at three axial locations: 0.2 m (top), 0.4 m (middle) and 0.6 m (bottom).

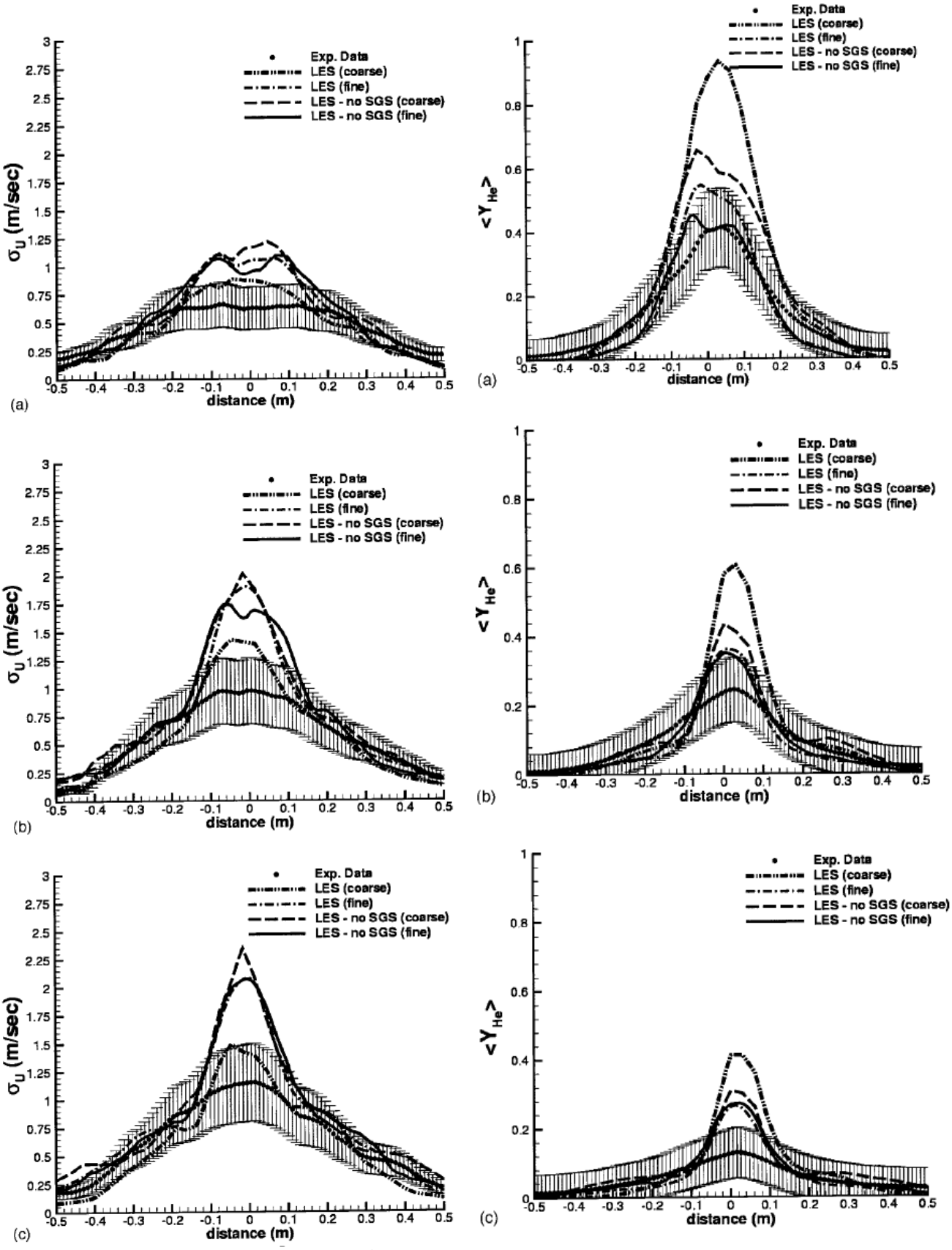

Figure 13 RMS axial velocity (left) and mean helium mass fractions (right) at three axial locations: 0.2 m (top), 0.4 m (middle) and 0.6 m (bottom).

The radial mean velocity predictions (Figure 12) show reasonable agreement with the experiments on the periphery of the plume but all of the simulations overpredict the radial velocity near the plume centreline. The best results are again achieved using the finer mesh.

RMS axial velocity profiles are shown in Figure 13. The coarse-grid results without the SGS model and the results on the fine grid with or without the SGS model all overpredict the RMS velocities by up to 75%. The best agreement is obtained with the coarse-grid using the SGS model. DesJardin *et al*. suggested that the relatively good performance for this last case is purely fortuitous and is due to excessive damping of the turbulent fluctuations. The generally poor predictions of the RMS velocity was attributed to under-resolution of the turbulent production and destruction near the base of the plume, resulting in an overly-coherent puffing motion. Radial RMS velocities (not shown) were better predicted, with fine-grid simulations falling within the experimental uncertainty bounds.

Figure 13 also shows the predicted and experimental mean helium mass fractions at the three downstream positions. The best predictions were obtained using the fine mesh without the SGS model, which were within the experimental uncertainty bounds for the two positions nearest the plume source. The worst results were obtained using the coarse-grid with the SGS model which overpredicted the experimental values by nearly a factor of two. The mean helium concentration decayed faster in the experiments than in the simulations, producing worsening agreement between experiments and simulations with increasing distance from the source.

DesJardin *et al*. [1] also presented predicted RMS concentration fluctuations which showed significant grid sensitivity and poor overall agreement with the experiments (errors of up to 200%). This was attributed to the sensitivity of the concentration fluctuations to the small scales of motion that were not resolved by the LES. They suggested that the RMS velocity fluctuations did not show the same degree of sensitivity due to the smoothing effect of the pressure gradient in the momentum equation. The poor prediction of the concentration fluctuations has important implications for fire simulations, where the mixing of fuel and air determines the overall heat release rate.

4.2 Comparison of Tieszen et al. CFD Calculations with Experiments

Tieszen *et al*. [2] performed grid sensitivity tests using three different meshes, with 0.25M, 1M and 4M nodes. As the mesh density was increased, the amount of air entrained into the plume increased, which increased the centreline density. The best agreement between the CFD predictions and the experimental data was obtained using the finest mesh (see Figures 15 and 16). Analysis of the CFD results indicated that underprediction of entrainment with coarse grids was related to overprediction of the axial velocity near the plume source. Surprisingly, the mean radial velocity did not show significant sensitivity to the grid density. Coarse grids were found to produce overly-high resolved turbulent kinetic energy along the plume centreline, i.e. puffs that were too strong. Tieszen *et al*. [2] commented that this finding was consistent with a lack of mixing associated with plume puffing that was overly coherent (i.e. a lack of interaction between small and large scales).

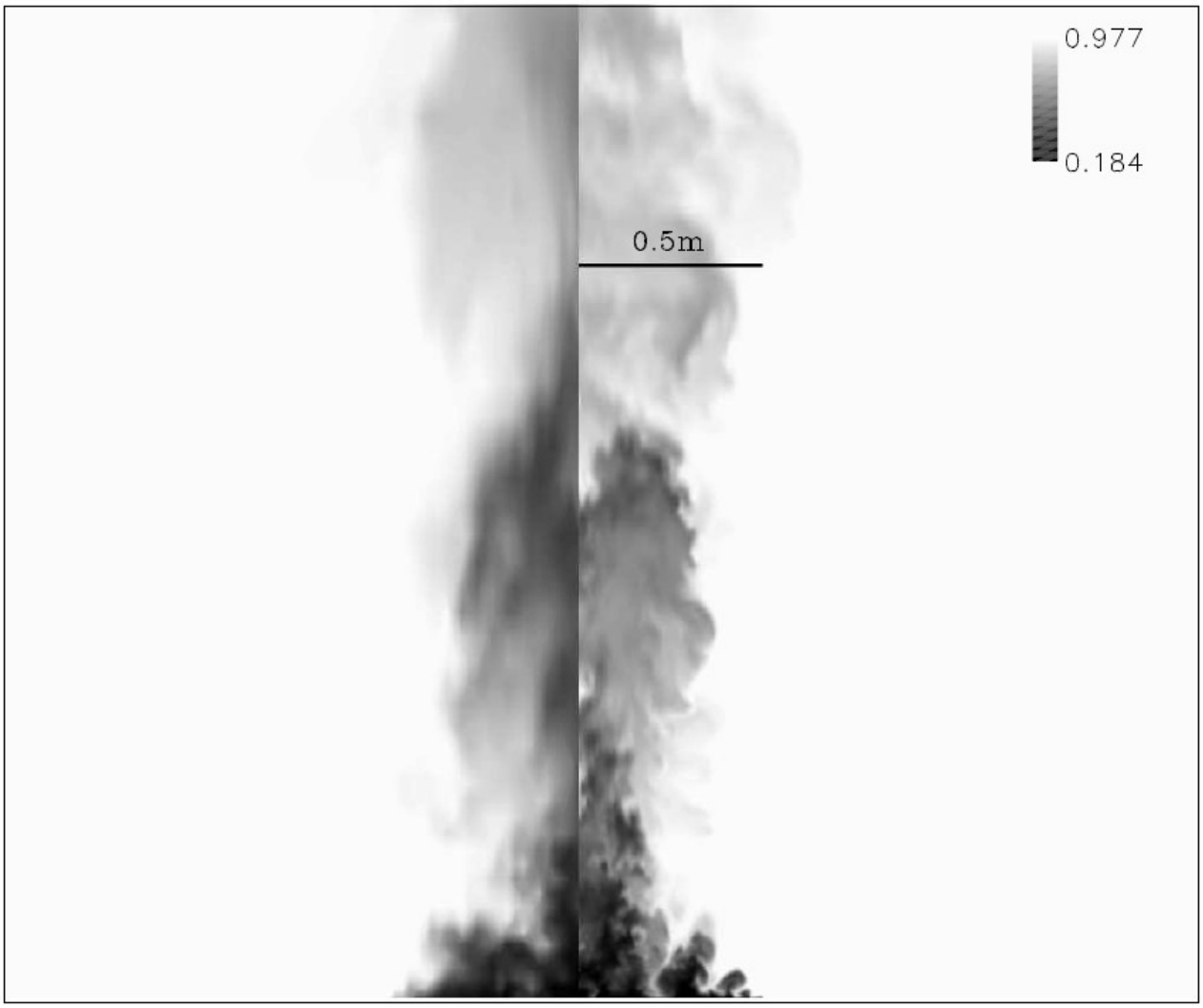

Figure 14 Instantaneous density contours with the 250k node mesh (left) and 4M node mesh (right), from Tieszen *et al*. [2].

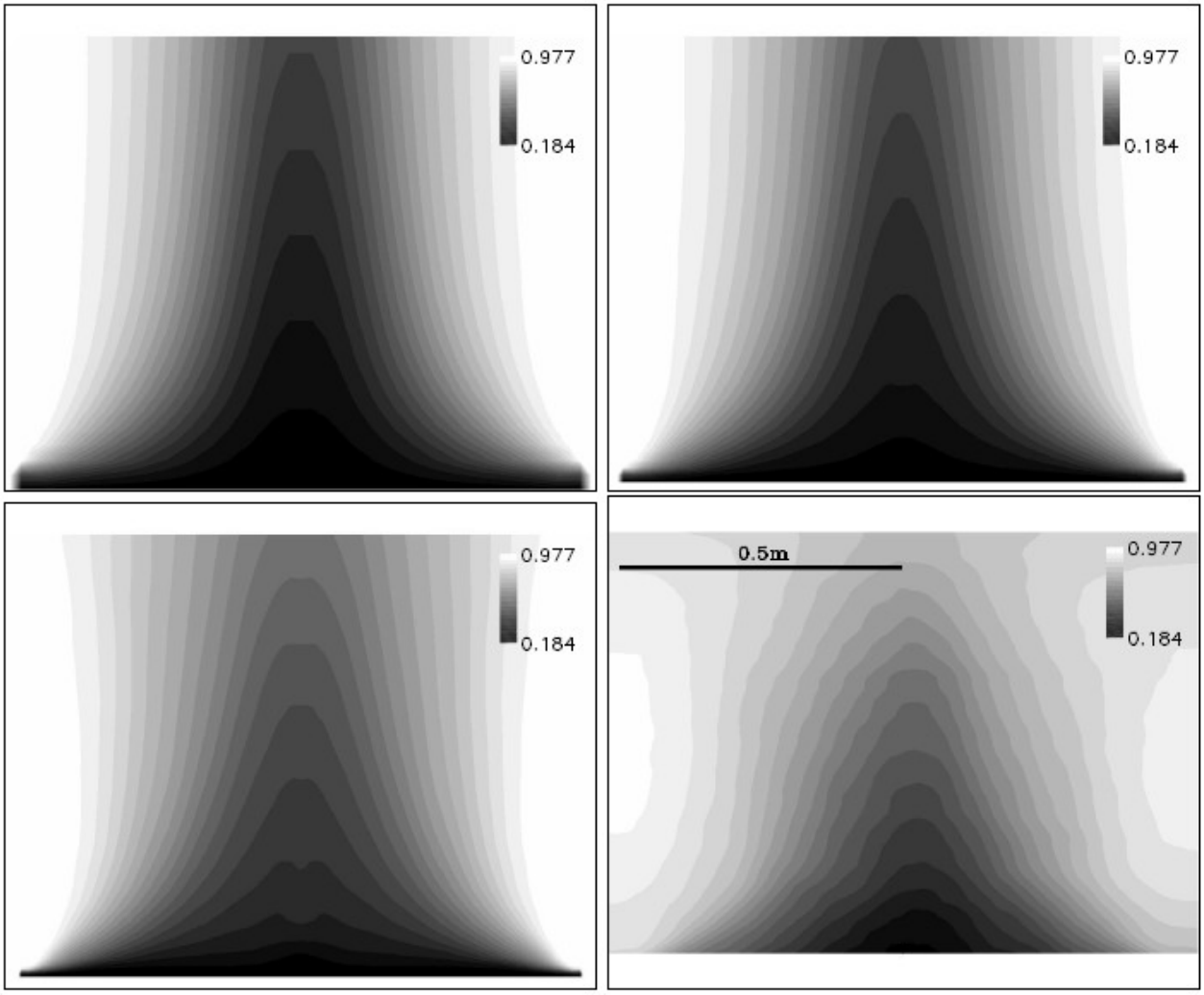

Figure 15 Mean density contours: simulations with 250k nodes (upper-left), 1M nodes (upper-right) and 4M nodes (lower-left); experiments (lower-right). From Tieszen *et al*. [2].

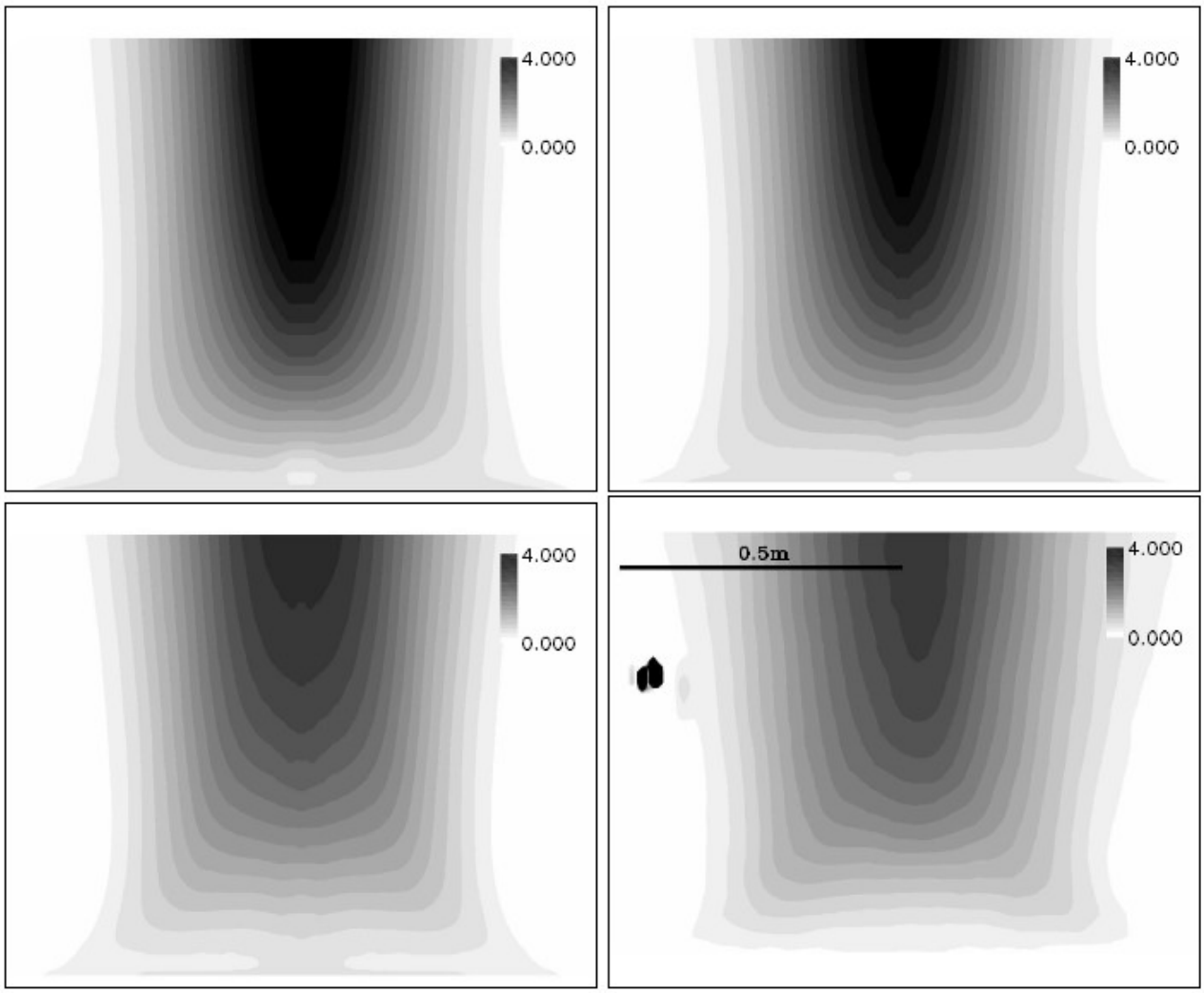

Figure 16 Mean axial velocity contours (in m/s): simulations with 250k nodes (upper-left), 1M nodes (upper-right) and 4M nodes (lower-left); experiments (lower-right). From Tieszen *et al*. [2].

4.3 Comparison of Xin [3] CFD Calculations with Experiments

In the simulations of Xin [3], the mean axial velocity was overpredicted at all measurement positions (Figure 17). The error increased with distance from the nozzle, approaching a factor of nearly 2 at $x/D = 0.8$. This behaviour is consistent with the findings of Tieszen *et al*. [2] and Chung & Devaud [39], that relatively coarse meshes lead to overprediction of the axial velocity. Significantly better mean velocity predictions were obtained by Chung & Devaud [39] using the same code with grid cells half the width.

The results from simulations undertaken with and without the baroclinic torque term showed that the mean axial velocity increased slightly when the term was included (Figure 17). This coincided with an increase in radial velocity close to the base of the plume. Neglecting the baroclinic torque produced lower helium mass fractions (Figure 18). The experimental mass fraction values were not shown for comparison in Xin's paper. Comparing instead with the results shown in DesJardin *et al*. [1] (see Figure 13), it appears that the mean concentrations decayed faster in the experiments than in the simulations. Overall, the results without the baroclinic torque were probably closer to the experiments than those with the term.

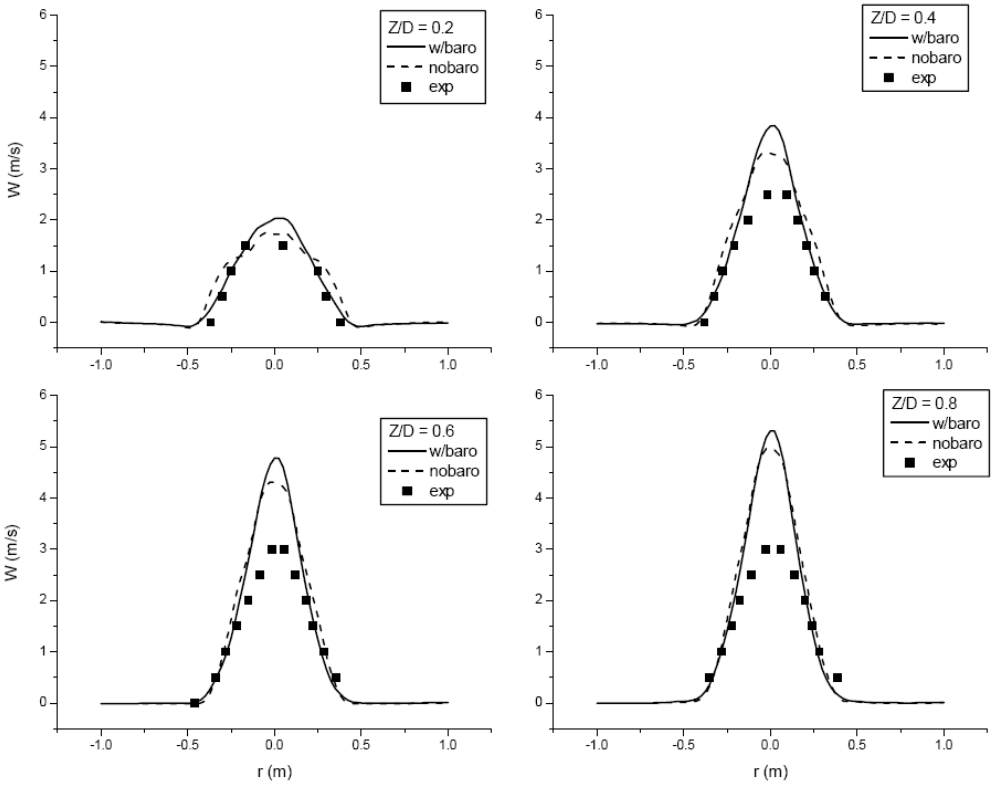

Figure 17 Predicted mean axial velocity at four axial positions obtained by Xin [3] using FDS with and without the baroclinic torque term.

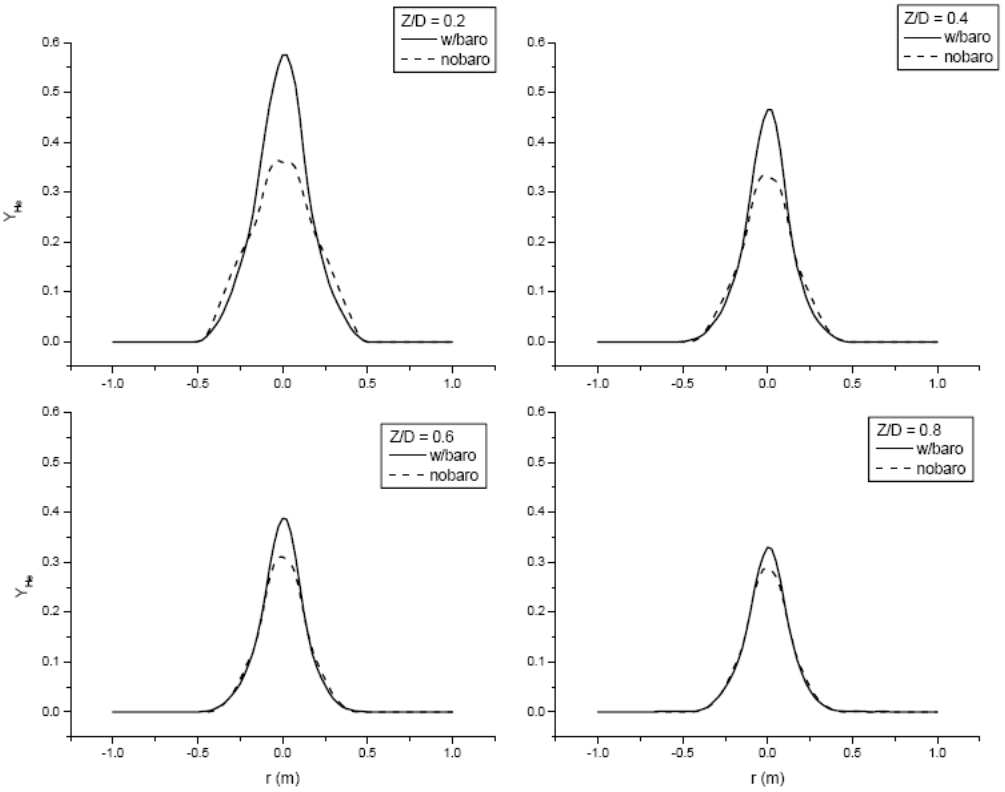

Figure 18 Predicted helium mass fractions at four axial positions obtained by Xin [3] using FDS with and without the baroclinic torque term.

4.4 Summary

Overall, the work of DesJardin *et al*. [1] is encouraging in showing that the mean axial velocity and concentration, and the puffing frequency of a turbulent plume can be predicted to a reasonably good degree of accuracy with a sufficiently fine mesh. Their results for the fine-grid (2.5M nodes) and no SGS model were for the most part within experimental uncertainty bounds. The fact that the results were better without an SGS model than with an SGS model suggests that there was still too much artificial damping at this resolution. This appears to be confirmed by the later study of Tieszen *et al*. [2] who obtained good experimental agreement in mean quantities using a 4M node grid with an SGS model. Further model assessment has shown that grids with at least 75 cells across the base of the plume are necessary to obtain mean velocity predictions in good agreement with the experiments[12].

Fluctuations of velocity and to a greater extent concentration were relatively poorly predicted in DesJardin *et al*.'s study and were very sensitive to the grid resolution. Better results were obtained using a finer uniform grid of 33M cells by Chung & Devaud [39] and with the non-uniform 2.3M grid used by Blanquart & Pitch [40], in which cells were clustered in the central plume region. In these two studies, the RMS velocity fluctuations were mostly within the limits of the experimental uncertainty. However, there were still differences in the RMS helium mass fraction predictions approaching a factor of two in some locations.

Grids of this size require fairly long computing times unless significant use can be made of parallel processors. For the 33M cell simulations, Chung & Devaud [39] found that simulations took just over two days using 16 Xeon processors. For industrial CFD applications which may also include further complexities in addition to the plume, such as flow impingement and boundary layers, the simulations will tend towards the upper limit of what can be achieved in practice.

DesJardin *et al*. [1] and Tieszen *et al*. [2] suggested that the cause of the poor fluctuation predictions and the need to use fine grids reflects the fact that the flow is driven primarily by density gradients, and close to the base of the plume these density gradients are very sharp. Furthermore, the small-scale turbulent structures near the plume source are not solely dissipating energy. The flow in this region does not follow the standard energy cascade from large to small eddies. Instead, the small structures comprise helium-bubbles and air-spikes induced by the Rayleigh-Taylor instability which are responsible for drawing air close into the plume source and help to break up the larger-scaled “puffing” flow structures related to the roll-up vortex. If these small structures are not well-resolved, the mean plume centreline density is too low and the centreline vertical velocity too high. The larger-scaled puffing motion does not require such a fine grid to be well resolved. For this reason, using coarse grids the puffing frequency can be well-captured, even though the small-scale mixing and the mean velocity and concentration may be poorly predicted.

The results from the simulations demonstrated that coarse meshes lead to overprediction of peak axial velocities and underprediction of the mean density. The turbulent kinetic energy is also overpredicted due to a lack of small (under-resolved) scales interacting with the larger coherent eddy flow structures. To obtain improved flow predictions without recourse to very fine meshes it is necessary to use an SGS model which accounts for the effects of the unresolved Rayleigh-Taylor instabilities and the net upscale transfer of turbulent energy. Recent simulations by Burton [41] using the nLES model have shown promising results in this respect.

12 *Tieszen, Personal Communication, 2010.*

5 Best Practice Advice for the UFR

5.1 Key Physics

The key physics of this UFR is the transient, unsteady behaviour in the near-field of a turbulent buoyant helium-air plume. The flow features two key instabilities. Firstly, the Rayleigh-Taylor instability related to the presence of dense fluid above less-dense fluid, which gives rise to fingers or spikes of dense fluid separated by rising bubbles of lighter fluid. Secondly, the Kelvin-Helmholtz instability related to the shear-layer interface between the rising plume and the ambient fluid, which produces roll-up vortex sheets on the boundary between the two layers of fluid travelling at different velocities. The flow is very challenging to predict using CFD, due to the sharp density gradients at the plume exit which produce flow conditions where small scales of turbulent motion feed into the larger scales.

5.2 Numerical Modelling Issues

- For LES, the flow cannot be treated as two-dimensional or axisymmetric. Full three-dimensional time-dependent simulations must be performed.

- For simulation of the selected UFR test case, open boundaries should be used on all sides of the flow domain except for the floor. Constant pressure boundaries may be used, although if a fully-compressible code is used, care will need to be taken to ensure that the boundaries are non-reflective.

- For simulation of the selected UFR test case, the domain should extend at least 4 metres radially and vertically to minimize any effects of the open boundaries on the development of the plume. Ideally, tests should be performed to ensure that the location of the open boundaries has no significant effect on the results.

- The finest mesh should be used given the available computing resources. The results discussed above suggest that a mesh of around 4 million nodes should give good agreement with the experiments in terms of mean flow quantities, but may still be insufficient for good predictions of fluctuations or RMS values. Tieszen[13] noted that at least 75 cells across the base diameter of the plume are necessary to avoid significant differences in the vertical centreline velocity compared to the measured values. Ideally, a grid-dependence study should be undertaken to investigate the magnitude of these effects.

5.3 Physical Modelling

- Either the fully-compressible or the low-Mach-number form of the Navier-Stokes equations can be used. The fully-compressible N-S equations require more careful treatment to avoid acoustic waves reflecting back into the domain from open boundaries. Furthermore, they will require a very short time-step, based on the speed of sound instead of the local flow speed, unless special treatments are used. For details of a fully-compressible N-S treatment, see DesJardin *et al*. [1].

13 S. Tieszen, Private Communication, March 2010.

- The baroclinic torque is non-zero and therefore should not be neglected.

- The Boussinesq approximation, where flow properties are assumed not to vary as a function of temperature or composition, and where buoyancy is only included as an additional body-force term in the momentum equations, should not be used. The Boussinesq approximation is only appropriate for modelling small density differences, equivalent to a temperature difference less than around 15 °C in air [80].

- If an LES approach is used, the effect of the unresolved small-scale turbulence on the resolved motion can either be accounted for by an explicit sub-grid-scale model, such as the dynamic Smagorinsky model, or by numerical damping in an implicit LES (a "no-model" approach). If an explicit approach is taken, central differencing should ideally be used for convection in the momentum equation but bounded upwind-biased schemes will probably be needed for the scalar equations to prevent unbounded under/overshoots. DesJardin *et al*. [1] obtained slightly better results with the implicit approach but this is likely to depend on grid resolution. If a coarse grid is used, an explicit LES model should probably be avoided. Both implicit and explicit approaches should ideally be tested to examine the sensitivity of results to the turbulence treatment. Recent work by Blanquart & Pitsch [40] has shown very good predictions for both mean momentum and concentration using the Lagrangian dynamic SGS model of Meneveau *et al*. [51] for turbulent diffusion terms in both the momentum and helium mass-fraction transport equations.

- It is difficult to provide definitive guidance on use of RANS models, since to date it appears that there have only been two relevant studies for this flow, and they produced somewhat contradictory results. Chung & Devaud [39] found in the helium plume experiments of O'Hern *et al*. [4] that steady flow behaviour was obtained using $k - \varepsilon$ models with SGDH or GGDH and values of the model constant $C_{\varepsilon 3}$ varying between 0 and 1. They also found that assuming the flow to be axisymmetric or using a fully three-dimensional approach gave practically identical results and an axisymmetric approach with 22,882 cells gave a grid-independent solution. In contrast, Nicolette *et al*. [38] found a "standard" $k - \varepsilon$ model produced unsteady flow behaviour using all but the very coarsest of meshes, which had only 56,000 cells for the three-dimensional geometry. For meshes containing 500,000 to 2 million cells, the predicted flow behaviour was unsteady with the finer meshes resolving an increasing proportion of the unsteady flow structures. These differences in resolving steady or unsteady flow behaviour could in part be due to the former study using a steady solution method whilst the latter used a transient time-stepping approach. Nevertheless, Chung & Devaud [39] reported that the residuals in their steady simulations could be reduced to low levels (maximum residuals of 10^{-5}), whilst usually in flows where there is a tendency towards transient behaviour it is usually difficult to obtain such good convergence.
  Putting these differences to one side, the Chung & Devaud [39] study showed that good predictions of the steady flow behaviour in the near-field of buoyant plumes could be achieved provided that special care was taken over the choice of the model constant, $C_{\varepsilon 3}$. Different optimum values of $C_{\varepsilon 3}$ were found when using either SGDH or GGDH, and varying the value of $C_{\varepsilon 3}$ produced very marked changes in the flow predictions. It is highly recommended therefore if studying the near-field flow behaviour of plumes using similar models to examine the sensitivity of the results to this parameter.
  The Nicolette *et al*. [38] study mainly focused on testing their newly-developed Buoyant Vorticity Generation (BVG) extension to the $k - \varepsilon$ model. The model showed promising results in comparison to the helium plume experiments from NIST [31][32] and the Sandia FLAME facility with a low helium inlet velocity of 0.13 m/s. However, the model gave less

encouraging predictions when compared to the O'Hern *et al*. [4] experiments where the inlet velocity was higher, due to the delayed predicted onset of laminar to turbulent transition. There were also additional complications with mesh-dependent transient behaviour, as mentioned above.
Overall, the two studies indicate that further work is needed before definitive best-practice advise can be provided on the use of RANS models in the near-field of buoyant plumes.

The above comment address the use of LES and RANS models in the near-field region, up to around five diameters downstream from the source. LES predictions of the fully-developed plume in the far-field are presented by Zhou *et al*. [45][46] and Pham *et al*. [50]. For information on best-practice modelling of the steady far-field behaviour of buoyant plumes, see the companion UFR.

5.4 Application Uncertainties

- The mean velocity of the helium gas mixture flowing through the 1-metre-diameter inlet was different according to whether the value was Favre- or Reynolds-averaged. In the former case it was 0.339 m/s and in the latter case it was 0.325 m/s.

- The mean inlet helium and air temperatures in the experiments were slightly different, 11 °C and 13 °C, respectively. However the change in density associated with the 2 °C temperature difference is very small in comparison to that associated with the difference in the molecular weight of the helium mixture and air. The flow can therefore be treated as isothermal, at approximately 12 °C.

- The plume experiments involved the release of a helium, acetone and oxygen gas mixture with a molecular weight of 5.45 g/mol, rather than a pure helium with a molecular weight of 4.0 g/mol.

- Turbulence levels in the flow issuing from the 1-metre-diameter inlet and in the surrounding entrained air flow were not directly measured in the experiments. However, flow visualization strongly suggested the conditions in the helium inlet were laminar, and there was only weak turbulence in the entrained air. O'Hern *et al*. [4] considered that transition to turbulence in the plume was not driven by residual vorticity from the boundary layers in the inlet flows but instead came from gravitational and baroclinic torque in the plume. This was confirmed by DesJardin *et al*. [1], who found that superimposing turbulent fluctuations on the inlet velocity in their simulations did not affect the resulting predicted flow behaviour.

- The experiments were carefully designed to mimic conditions where the plume is unconfined and surrounded at the source by an infinite flat ground plane [4]. Measurements were undertaken to ensure the uniformity of the flow through the annular air inlet into the chamber and the facility was designed following extensive CFD modelling studies to eliminate any disturbances to the plume. Without models reproducing exactly the same geometry as used in the experiments this remains a potential source of uncertainty. Whilst the majority of the published studies have chosen to simulate an unconfined plume on a flat plane, Chung & Devaud [39] and Blanquart & Pitsch [40] both modelled the complete geometry.

- There are some discrepancies in the boundary conditions used by DesJardin *et al*. [1]. The

plume experiments involved the release of a helium, acetone and oxygen gas mixture with a molecular weight of 5.45 g/mol, whereas DesJardin *et al.* instead modelled a pure helium plume with a molecular weight of 4.0 g/mol. They also used an inlet velocity of 0.351 m/s whereas the inlet Favre-averaged velocity measured in the experiments was 0.339 m/s [4]. Furthermore, DesJardin *et al*. [1] used a small co-flow velocity of 0.01 m/s around the plume source whereas the velocity in the experiments was zero, due to the presence of the 0.51 m wide steel plate. The simulations presented DesJardin *et al*. [1] were carried out at the same time as the experiments based on an initial design, and there was insufficient time to repeat the CFD simulations once the experimental conditions were fully established[14]. Due to these differences, there remains some uncertainty in the model predictions.

- It is considerably more challenging to establish grid-independence for LES than it is for traditional RANS simulations. Grid independence can only ever be achieved for statistical quantities, such as mean velocities and Reynolds stresses, and not for the instantaneous field, which will change with grid resolution [83]. Unlike RANS, it is usually not possible to separate the effects of the turbulence model and the discretization errors. Most commercial CFD codes use implicit filtering, whereby discretization of the governing equations is assumed to act as a filtering process. The filter width, Δ, in the SGS model is then usually taken as the cube-root of the cell volume (or twice the cube-root in some codes). The turbulence model is therefore intrinsically linked to the grid resolution: refining the grid affects both the discretization errors and the turbulence model itself[15]. In theory, a truly grid-independent solution could be obtained by refining the grid to the point where the solution becomes effectively a DNS, or by using an alternative approach based on explicit filtering, which separates the discretization errors from the SGS modelling effects (see for example Gullbrand & Chow [84]). However, these approaches are costly and are rarely used in practice. Consequently, most LES solutions use implicit filtering and the solutions often involve a complex mixture of numerical and modelling errors. The interaction between these errors has been studied by Geurts *et al*. [85][86][81], who found that in some flows their interaction can actually lead to results becoming worse as the grid is refined. They suggested that it may be more effective to run a number of simulations with relatively coarse meshes to help understand the grid-dependence issues and optimize the SGS model coefficients, rather than run just one or two simulations using the finest mesh possible (see also Klein *et al*. [87] [88]). Their studies have so far been limited to relatively simple flows, such as homogeneous isotropic turbulence. In the plume studies presented here, there appears to be a consistent trend for results to improve as the grid is made progressively finer. This appears to be due to key physical processes controlling the development of turbulent structures in plumes being present only in the very small scales. The need for a very fine grid to resolve the Rayleigh-Taylor instabilities in plumes is discussed in some detail in DesJardin *et al*. [1] and Tieszen *et al*. [2], and is summarized above. This matter introduces uncertainties for industrial LES practitioners seeking to reproduce the results from the above plume studies using their own commercial or in-house CFD codes that rely on different numerical schemes and meshing practices. Although various measures have been proposed to indicate whether the LES grid is sufficiently fine, such as the LES Index of Quality of Celik *et al*. [89][90], these are still the subject of ongoing research and have yet to proven widely applicable in practice [91].

- The usefulness of the QNET UFR's is to provide best-practice guidance for CFD simulations

14 *DesJardin, Personal Communication, 2010.*

15 This should not be confused with the MILES approach [82], where the numerical scheme is devised to account for the effects of the unresolved turbulence and there is no explicit SGS model, although the same considerations apply.

of various different generic flows. It is important that the guidance is *general* rather than being specific to just one particular set of experiments. With this in mind for the present UFR, it is perhaps worthwhile reflecting on the differences between non-reacting helium plumes and fire plumes to help identify possible uncertainties that may arise in extrapolating the advice from this UFR to the modelling of fire plumes. In helium plumes the strongest gradients are at the base of the plume and the mean driving force decreases with height. In fire plumes, however, due to combustion being dependent upon fuel and air mixing, the driving force first increases with height as the combustion rate increases and only further downstream starts decreasing. Most fuel vapours are denser than air and produce a fuel core or vapour dome around the source [42]. They may not therefore be subject to the same Rayleigh-Taylor instabilities that occur in helium plumes. This suggests that to model fires, it may not be necessary to model the bubble and spike structures that are important in helium plumes and grid dependence may be less of an issue. Further work is necessary to confirm this.

5.5 Recommendations for Future Work

Whilst the studies discussed in this UFR provide some guidance on appropriate grid resolution for the O'Hern *et al*. [4] helium plume, it is difficult to formulate generic rules from this for other plumes involving for example different density ratios, Richardson and Reynolds numbers. Such guidance would be extremely welcome in the industrial CFD community where studies are often made of flows where there is no experimental data available and where CFD models are used as truly predictive tools.

The discussion of grid-dependence issues in the works of Tieszen *et al*. [2][42] suggests two possible criteria that could be investigated in future work to help formulate guidance on grid-resolution for LES simulations of plumes. In [2], the characteristic length scale of the Rayleigh-Taylor instability is estimated as:

$$\lambda = \left(\frac{D^2}{A\,g} \right)^{1/3} \tag{20}$$

where D is the diffusion coefficient between plume and air, A is the Atwood number (the density difference divided by the sum of the densities) and g is the gravitational acceleration. A possible rule for grid refinement could be based on the local grid size as a function of λ in much the same way that Baggett *et al*. [92] suggest that the grid size should be a certain fraction of the integral length scale (see also [93]).

Secondly, Tieszen *et al*. [42] noted that simulations with fine meshes resolved the air-spike structures characteristic of the Rayleigh-Taylor instability but coarse-grid simulations did not. A second measure could therefore be based on the appearance (or not) of air spike structures in the simulations. Clearly it would be necessary beforehand to have some physical criteria for the actual appearance of air spikes in real plumes, perhaps based on the Reynolds, Froude or Richardson number, or the width of the plume source (see discussion in Section 2.2).

It would be useful to investigate further the performance of steady and unsteady RANS models in predicting the near-field behaviour of turbulent plumes, in particular algebraic and differential stress models. The only relevant studies to date appears to be the work the works of Nicolette *et al*. [38] and Chung & Devaud [39], who tested variants of the k–ε model.

Finally, further well-instrumented and carefully controlled experiments would be welcome for industrially-relevant turbulent plumes. This would preferably be combined with a cohort of CFD studies where different CFD models and numerical methods are compared to experimental data.

Bibliography

1. DesJardin, P. E., O'Hern, T. J. and Tieszen, R., Large eddy simulation and experimental measurements of the near-field of a large turbulent helium plume, *Phys. Fluids*, 16, p.1866-1883, 2004
2. Tieszen, S. R., Pitsch, H., Blanquart, G. and Abarzhi, S., Toward the development of a LES-SGS closure model for buoyant plumes, in *Proc. of the Summer Program*, *Center for Turbulence Research, Stanford*, 2004
3. Xin, Y., Baroclinic effects on fire flow field, in *Proc. 4th Joint Meeting of the U.S. Section of the Combustion Institute*, Philadelphia, PA, 2005
4. O'Hern, T. J., Weckman, E. J., Gerhart, A. L., Tieszen, S. R. and Schefer, R. W., Experimental study of a turbulent buoyant helium plume, *J. Fluid Mech.*, 544, p.143-171, 2005
5. Chen, C. J. and Rodi, W., *Vertical buoyant jets: a review of experimental data*, Pergamon, New York, 1980
6. List, E. J., Turbulent jets and plumes, *Ann. Rev. Fluid Mech.*, 14, p.189-212, 1982
7. List, E. J., Mechanics of turbulent buoyant jets and plumes, in *Turbulent Buoyant Jets and Plumes*, Rodi, W. (Ed.), Pergamon Press, 1982
8. Drysdale, D., *An introduction to fire dynamics*, John Wiley & Sons, 1998
9. Dimonte, G., Youngs, D. L., Dimits, A., Weber, S., Marinak, M., Wunsch, S., Garasi, C., Robinson, A., Andrews, M. J., Ramaprabhu, P., Calder, A. C., Fryxell, B., Biello, Dursi, L., MacNeice, P., Olson, K., Ricker, P., Rosner, R., Timmes, F., Tufo, H., Young, Y.-N. And Zingale, M., A comparative study of the turbulent Rayleigh-Taylor instability using high-resolution three-dimensional numerical simulations: The Alpha-Group collaboration, *Phys. Fluids*, 16, p.1668-1693, 2004
10. Cook, A. W. and Dimotakis, P. E., Transition stages of Rayleigh-Taylor instability between miscible fluids, *J. Fluid Mech.*, 457, p.69-99, 2002
11. Jacobs, J. W. and Dalziel, S. B., Rayleigh-Taylor instability in complex stratifications, *J. Fluid Mech.*, 542, p.251-279, 2005
12. Cabot, W. H., Cook, A. W., Miller, P. L., Laney, D. E., Miller, M. C. and Childs, H. R., Large-eddy simulation of Rayleigh-Taylor instability, *Phys. Fluids*, 17, DOI: 10.1063/1.1942519, 2005
13. Cook, A. W., Cabot, W. and Miller, P. L., The mixing transition in Rayleigh-Taylor instability, *J. Fluid Mech.*, 511, p.333-362, 2004
14. Buckmaster, J. and Peters, N., The infinite candle and its stability - a paradigm for flickering diffusion flames, in *Proc. 21st Symposium (International) on Combustion*, The Combustion Institute, Pittsburgh, PA, 1986
15. Ghoniem, A. F., Lakkis, I. and Soteriou, M., Numerical simulation of the dynamics of large fire plumes and the phenomenon of puffing, in *Proc. 26th Symposium (International) on Combustion*, The Combustion Institute, Pittsburgh, PA, 1996
16. Coats, C. M., Coherent structures in combustion, *Prog. Energy Combust. Sci.*, 22, p.427-509, 1996
17. Albers, B. W. and Agrawal, A. K., Schlieren analysis of an oscillating gas-jet diffusion

flame, *Combust. Flame*, 119, p.84-94, 1999

18. Cetegen, B. M. and Kasper, K. D., Experiments on the oscillatory behavior of buoyant plumes of helium and helium-air mixtures, *Phys. Fluids*, 8, p.2974, 1996
19. Gebhart, B., Jaluria, Y., Mahajan, R. L. and Sammakia, B., *Buoyancy-induced flows and transport*, Hemisphere Pub. Corp., New York, 1988
20. Juang, X. and Luo, K. H., Spatial direct numerical simulation of the large vortical structures in forced plumes, *Flow Turbul. Combust.*, 64, p.43-69, 2000
21. Jiang, X. and Luo, K. H., Direct numerical simulation of the puffing phenomenon of an axisymmetric thermal plume, *Theoret. Comput. Fluid Dynamics*, 14, p.55-74, 2000
22. Subbarao, E. R. and Cantwell, B. J., Investigation of a co-flowing buoyant jet: experiments on the effect of Reynolds number and Richardson number, *J. Fluid Mech.*, 245, p.69-90, 1992
23. Cetegen, B. M., Dong, Y. and Soteriou, M. C., Experiments on stability and oscillatory behavior of planar buoyant plumes, *Phys. Fluids*, 10, p.1658-1665, 1998
24. Soteriou, M. C., Dong, Y. and Cetegen, B. M., Lagrangian simulation of the unsteady near field dynamics of planar buoyant plumes, *Phys. Fluids*, 14, p.3118-3140, 2002
25. Cetegen, B. M. and Ahmed, T. A., Experiments on the periodic instability of buoyant plumes and pool fires, *Combust. Flame*, 93, p.157, 1993
26. Hamins, A., Yang, J. C. and Kashiwagi, I., An experimental investigation of the pulsation frequency of flames, in *Proc. 24th Symposium (International) on Combustion*, The Combustion Institute, Pittsburgh, PA, 1992
27. Kyle, D. M. and Sreenivasan, K. R., The instability and breakdown of a round variable density jet, *J. Fluid Mech.*, 249, p.619-664, 1993
28. Cetegen, B. M., Behavior of naturally unstable and periodically forced axisymmetric buoyant plumes of helium and helium-air mixtures, *Phys. Fluids*, 9, p.3742-3752, 1997
29. Cetegen, B. M. and McTeague, J., Behavior of periodically forced buoyant plumes, in *National Institute of Standards and Technology Annual Conference on Fire Research*, Gaithersburg, MD, October 28-31, 1996
30. Cetegen, B. M., Measurements of instantaneous velocity field of a non-reacting pulsating buoyant plume by Particle Image Velocimetry, *Combust. Sci. Technol.*, 123, p.377-387, 1997
31. Mell, W. E., Johnson, A., McGrattan, K. B. and Baum, H. R., Large eddy simulations of buoyant plumes, in *Chemical & Physical Processes in Combustion, Proc. Fall Technical Meeting*, 1995
32. Mell, W. E., McGrattan, K. B. and Baum, H. R., Numerical simulation of combustion in fire plumes, in *Proc. 26th Symposium (International) on Combustion*, The Combustion Institute, Pittsburgh, PA, 1996
33. Yep, T.-W., Agrawal, A. K. and Griffin, D., Gravitational effects on near-field flow structure of low-density gas jets, *AIAA J.*, 41, p.1973-1979, 2003
34. Pasumarthi, K. S. and Agrawal, A. K., Buoyancy effects on flow transition in low-density inertial gas jets, *Experiments in Fluids*, 38, p.541-544, 2005
35. Pera, L. and Gebhart, B., On the stability of laminar plumes: some numerical solutions and

experiments, *Int. J. Heat Mass Transfer*, 14, p.975-984, 1971

36. Gebhart, B., Instability, transition and turbulence in buoyancy-induced flows, *Annu. Rev. Fluid Mech.*, 5, p.213-246, 1973

37. O'Hern, T. J., Tieszen, S. R., Weckman, E. J., Gerhart, A. L. and Schefer, R. W., Simultaneous cinematographic PIV and acetone PLIF for spatially and temporally resolved velocity and concentration fields in a buoyant helium plume, in *Proc. ASME Int. Mech. Eng. Congress & Exposition*, ASME Fluids Engineering Division, 2001

38. Nicolette, V. F., Tieszen, S. R., Black, A. R., Domino, S. P. and O'Hern, T. J., A turbulence model for buoyant flows based on vorticity generation, *Sandia Report SAND2005-6273*, October, 2005

39. Chung, W. and Devaud, C. B., Buoyancy-corrected k-ε models and large eddy simulation applied to a large axisymmetric helium plume, *Int. J. Num. Meth. Fluids*, 58, p.57-89, 2008

40. Blanquart, G. and Pitsch, H., Large-eddy simulation of a turbulent buoyant helium plume, *Annual Research Briefs*, Center for Turbulence Research, p.245-252, 2008

41. Burton, G. C., Large-eddy simulation of a turbulent helium-air plume using the nLES method, *Annual Research Briefs*, Center for Turbulence Research, p.261-271, 2009

42. Tieszen, S. R., Domino, S. P. and Black, A. R., Validation of a simple turbulence model suitable for closure of temporally-filtered Navier-Stokes equations using a helium plume, in *Report SAND2005-3210*, Sandia National Laboratories, Albuquerque, New Mexico, 2005

43. Lingens, A., Neemann, K., Meyer, J. and Schreiber, M., Instability of diffusion flames, in *Proc. 26th Symposium (International) on Combustion*, The Combustion Institute, Pittsburgh, PA, 1996

44. Lingens, A., Reeker, M. and Schreiber, M., Instability of buoyant diffusion flames, *Exp. Fluids*, 20, p.241-248, 1996

45. Zhou, X., Luo, K. H. and Williams, J. J. R., Large-eddy simulation of a turbulent forced plume, *Eur. J. Mech. B - Fluids*, 20, p.233-254, 2001

46. Zhou, X., Luo, K. H. and Williams, J. J. R., Study of density effects in turbulent buoyany jets using large-eddy simulation, *Theoret. Comput. Fluid Dynamics*, 15, p.95-120, 2001

47. George, W. K. Jr., Alpert, R. L. and Tamanini, F., Turbulence measurements in an axisymmetric buoyant plume, *Int. J. Heat Mass Transfer*, 20, p.1145-1154, 1977

48. Shabbir, A. and George, W. K., Experiments on a round turbulent buoyant plume, *J. Fluid Mech.*, 275, p.1-32, 1994

49. Zhou, X. and Hitt, D. L., Proper orthogonal decomposition analysis of coherent structures in a transient buoyant jet, *J. Turbulence*, 5, p.1-21, 2004

50. Pham, M. V., Plourde, F. and Doan, S., Direct and large-eddy simulations of a pure thermal plume, *Phys. Fluids*, 19, DOI: 10.1063/1.2813043, 1997

51. Meneveau, C., Lund, T. and Cabot, W., A Lagrangian dynamic subgrid-scale model of turbulence, *J. Fluid Mech.*, 319, p.353-385, 1996

52. Worthy, J. and Rubini, P. A., Large eddy simulation of buoyant plumes, in *Proc. 4th Int. Seminar on Fire & Explosion Hazards*, Londonderry, UK, 2003

53. Worthy, J. and Rubini, P., A study of LES stress and flux models applied to a buoyant jet, *Num. Heat Trans. Part B*, 48, p.235-256, 2005

54. Worthy, J., *Large eddy simulation of buoyant plumes*, PhD Thesis, School of Mech. Eng, Cranfield University, UK, 2003

55. Metais, O. and Lesieur, M., Spectral large eddy simulations of isotropic and stably-stratified turbulence, *J. Fluid Mech.*, 239, p.157-194, 1992

56. Schumann, U., Subgrid-scale model for finite-difference simulations in plane channels and annuli, *J. Comp. Phys.*, 18, p.376-404, 1975

57. Leonard, A., Energy cascade in large-eddy simulations of turbulent flows, *Adv. Geophys.*, 18, p.237-248, 1974

58. Bardina, J., Ferziger, J. H. and Reynolds, W. C., Improved subgrid scale models for large eddy simulations, in *AIAA Paper 80-1357*, 1980

59. Burton, G. C. and Dahm, W. J., Multifractal subgrid-scale modeling for large eddy simulation. Part I: Model development and *a priori* testing, *Phys. Fluids*, 17, 075111, 2005

60. Burton, G. C. and Dahm, W. J., Multifractal subgrid-scale modeling for large eddy simulation. Part II: Backscatter limiting and *a posteriori* evaluation, *Phys. Fluids*, 17, 075112, 2005

61. Kang, Y. and Wen, J. X., Large eddy simulation of a small pool fire, *Combust. Sci. and Tech.*, 176, p.2193-2223, 2004

62. Wen, J. X., Kang, K., Donchev, T. and Karwatzki, J. M., Validation of FDS for the prediction of medium-scale pool fires, *Fire Safety Journal*, 42, p.127-138, 2007

63. Bastiaans, R. J. M., Rindt, C. C. M., Nieuwstadt, F. T. M. and van Steenhoven, A. A., Direst and large-eddy simulation of the transition of two and three-dimensional plane plumes in a confined enclosure, *Int. J. Heat Mass Transfer*, 43, p.2375-2393, 2000

64. Blanchat, T. K., Characterization of the air source and plume source at FLAME, in *Report SAND2001-2227*, Sandia National Laboratories, Albuquerque, New Mexico, 2001

65. Germano, M., Piomelli, U., Moin, P. and Cabot, W. H., A dynamic subgrid scale eddy viscosity model, *Phys. Fluids A*, 3, p.1760-1765, 1991

66. Lilly, D. K., A proposed modification to the Germano subgrid-scale closure model, *Phys. Fluids A*, 4, p.633-635, 1992

67. Fureby, C., On subgrid scale modelling in large eddy simulations of compressible flow, *Phys. Fluids*, 8, p.1301-1311, 1996

68. Ragab, S. A. and Sheen, S., Large eddy simulation of a mixing layer, in *AIAA Paper 91-0233*, 1991

69. Ragab, S. A., Sheen, S. and Sreedhar, M., An investigation of finite difference methods for large eddy simulations of a mixing layer, in *AIAA Paper 92-0554*, 1992

70. O'Rourke, P. J. and Bracco, F. V., Two scaling transformations for the numerical computation of multidimensional unsteady laminar flames, *J. Comput. Phys.*, 33, p.184, 1979

71. Ramshaw, J. D., O'Rourke, P. J. and Stein, L. R., Pressure gradient scaling method for fluid dlow with nearly uniform pressure, *J. Comput. Phys.*, 58, p.360, 1985

72. Rudy, D. H. and Strikwerda, J. C., A nonreflecting outflow boundary condition for subsonic Navier-Stokes calculations, *J. Comput. Phys.*, 36, p.55-70, 1980

73. Rudy, D. H. and Strikwerda, J. C., Boundary-conditions for subsonic compressible Navier-

Stokes calculations, *J. Comput. Phys.*, 9, p.327-338, 1981

74. Ghosal, S., An analysis of numerical errors in large-eddy simulations of turbulence, *J. Comp. Phys.*, 125, p.187-206, 1996

75. Mittal, R. and Moin, P., Suitability of upwind-biased finite difference schemes for large-eddy simulation of turbulent flows, *AIAA J.*, 35, p.1415-1417, 1997

76. Pierce, C. D., *Progress-variable approach for large eddy simulation of combustion*, PhD Thesis, Dept. of Mech. Eng., Stanford University, California 2001

77. Pierce, C. D. and Moin, P., Progress-variable approach for large eddy simulation of non-premixed turbulent combustion, *J. Fluid Mech.*, 504, p.73-97, 2004

78. McGrattan, K., Fire Dynamics Simulator (Version 4): Technical Reference Guide, in *NIST Special Publication 1018*, Gaithersburg, MD, 2006

79. Geurts, B. J. and Frohlich, J., Numerical effects contaminating LES: a mixed story, in *Modern simulation strategies for turbulent flow*, B. J. Geurts (Ed.), R. T. Edwards Inc., 2001

80. Ferziger, J. H. and Peric, M., *Computational Methods for Fluid Dynamics*, Springer-Verlag, Berlin, 2004

81. Geurts, B. J., Interacting errors in large-eddy simulation: a review of recent developments, *J. Turbulence*, 7, DOI: 10.1080/14685240600796507, 2006

82. Boris, J. P., Grinstein, F. F., Oran, E. S. and Kolbe, R. L., New insights into Large Eddy Simulation, *Fluid Dyn. Res.*, 10, p.199-228, 1992

83. Pope, S. B., Ten questions concerning the large-eddy simulation of turbulent flows, *New Journal of Physics*, 6, p.1-24, 2004

84. Gullbrand, J. and Chow, F. K., The effect of numerical errors and turbulence models in large-eddy simulations of channel flow, with and without explicit filtering, *J. Fluid Mech.*, 495, p.323-341, 2003

85. Geurts, B. J., *Elements of direct and large-eddy simulation*, R. T. Edwards, 2003

86. Meyers, J., Geurts, B. J. and Baelmans, M., Optimality of the dynamic procedure for large-eddy simulation, *Phys. Fluids*, 17, 045108, 2005

87. Klein, M., An attempt to assess the quality of large eddy simulations in the context of implicit filtering, *Flow Turbulence and Combustion*, 75, p.131-147, 2005

88. Freitag, M. and Klein, M., An improved method to assess the quality of large eddy simulations in the context of implicit filtering, *J. Turbulence*, DOI 10.1080/14685240600726710, 2006

89. Celik, I. B., Klein, M., Freitag, M. and Janicka, J., Assessment measures for URANS/DES/LES: an overview with applications, *J. Turbulence*, DOI:10.1080/14685240600794379, 2006

90. Celik, I, Klein, M. and Janicka, J., Assessment measures for engineering LES applications, *J. Fluids Eng.*, DOI:10.1115/1.3059703, 2009

91. Gant, S. E., Reliability issues of LES-related approaches in an industrial context, *Flow, Turb. Combust.*, 84, p.325-335, 2009

92. Baggett, J. S., Jimenez, J. and Kravchenko, A. G., Resolution requirements in large-eddy simulations of shear flows, in *Annual Research Briefs, Center for Turbulence Research, Stanford*, 1997

93. Addad, Y., Benhamadouche, S. and Laurence, D., The negatively buoyant wall-jet: LES results, *Int. J. Heat Fluid Flow*, 25, p.795-808, 2004

Bibliography

IGNORE THE BIBLIOGRAPHY BELOW

1 DesJardin, P. E., O'Hern, T. J. and Tieszen, R., Large eddy simulation and experimental measurements of the near-field of a large turbulent helium plume, *Phys. Fluids*, 16, p.1866-1883, 2004

2 Tieszen, S. R., Pitsch, H., Blanquart, G. and Abarzhi, S., Toward the development of a LES-SGS closure model for buoyant plumes, in *Proc. of the Summer Program*, (Eds), , 2004

3 Xin, Y., Baroclinic effects on fire flow field, in *Proc. 4th Joint Meeting of the U.S. Section of the Combustion Institute*, (Eds), , 2005

4 O'Hern, T. J., Weckman, E. J., Gerhart, A. L., Tieszen, S. R. and Schefer, R. W., Experimental study of a turbulent buoyant helium plume, *J. Fluid Mech.*, 544, p.143-171, 2005

5 Chen, C. J. and Rodi, W., *Vertical buoyant jets: a review of experimental data*, Pergamon, New York,1980

6 List, E. J., Turbulent jets and plumes, *Ann. Rev. Fluid Mech.*, 14, p.189-212, 1982

7 List, E. J., Mechanics of turbulent buoyant jets and plumes, in *Turbulent Buoyant Jets and Plumes*, Rodi, W. (Eds), Pergamon Press, 1982

8 Drysdale, D., *An introduction to fire dynamics*, John Wiley & Sons, ,1998

9 Dimonte, G., Youngs, D. L., Dimits, A., Weber, S., Marinak, M., Wunsch, S., Garasi, C., Robinson, A., Andrews, M. J., Ramaprabhu, P., Calder, A. C., Fryxell, B., Biello, etc., A comparative study of the turbulent Rayleigh-Taylor instability using high-resolution three-dimensional numerical simulations: The Alpha-Group collaboration, *Phys. Fluids*, 16, p.1668-1693, 2004

10 Cook, A. W. and Dimotakis, P. E., Transition stages of Rayleigh-Taylor instability between miscible fluids, *J. Fluid Mech.*, 457, p., 2002

11 Jacobs, J. W. and Dalziel, S. B., Rayleigh-Taylor instability in complex stratifications, *J. Fluid Mech.*, 542, p., 2005

12 Cabot, W. H., Cook, A. W., Miller, P. L., Laney, D. E., Miller, M. C. and Childs, H. R., Large-eddy simulation of Rayleigh-Taylor instability, *Phys. Fluids*, 17, p., 2005

13 Cook, A. W., Cabot, W. and Miller, P. L., The mixing transition in Rayleigh-Taylor instability, *J. Fluid Mech.*, 511, p.333-362, 2004

14 Buckmaster, J. and Peters, N., The infinite candle and its stability - a paradigm for flickering diffusion flames, in *Proc. 21st Symposium (International) on Combustion*, (Eds), The Combustion Institute, Pittsburgh, PA, 1986

15 Ghoniem, A. F., Lakkis, I. and Soteriou, M., Numerical simulation of the dynamics of large fire plumes and the phenomenon of puffing, in *Proc. 26th Symposium (International) on Combustion*, (Eds), The Combustion Institute, Pittsburgh, PA, 1996

16 Coats, C. M., Coherent structures in combustion, *Prog. Energy Combust. Sci.*, 22, p.427-509, 1996

17 Albers, B. W. and Agrawal, A. K., Schlieren analysis of an oscillating gas-jet diffusion flame, *Combust. Flame*, 119, p.84-94, 1999

18 Cetegen, B. M. and Kasper, K. D., Experiments on the oscillatory behavior of buoyant plumes of helium and helium-air mixtures, *Phys. Fluids*, 8, p.2974, 1996

19 Gebhart, B., Jaluria, Y., Mahajan, R. L. and Sammakia, B., *Buoyancy-induced flows and transport*, Hemisphere Pub. Corp., New York,1988

20 Juang, X. and Luo, K. H., Spatial direct numerical simulation of the large vortical structures in forced plumes, *Flow Turbul. Combust.*, 64, p.43-69, 2000

21 Jiang, X. and Luo, K. H., Direct numerical simulation of the puffing phenomenon of an axisymmetric thermal plume, *Theoret. Comput. Fluid Dynamics*, 14, p.55-74, 2000
22 Subbarao, E. R. and Cantwell, B. J., Investigation of a co-flowing buoyant jet: experiments on the effect of Reynolds number and Richardson number, *J. Fluid Mech.*, 245, p.69-90, 1992
23 Cetegen, B. M., Dong, Y. and Soteriou, M. C., Experiments on stability and oscillatory behavior of planar buoyant plumes, *Phys. Fluids*, 10, p.1658-1665, 1998
24 Soteriou, M. C., Dong, Y. and Cetegen, B. M., Largrangian simulation of the unsteady near field dynamics of planar buoyant plumes, *Phys. Fluids*, 14, p.3118-3140, 2002
25 Cetegen, B. M. and Ahmed, T. A., Experiments on the periodic instability of buoyant plumes and pool fires, *Combust. Flame*, 93, p.157, 1993
26 Hamins, A., Yang, J. C. and Kashiwagi, I., An experimental investigation of the pulsation frequency of flames, in *Proc. 24th Symp. Int. on Combustion*, (Eds), , 1992
27 Kyle, D. M. and Sreenivasan, K. R., The instability and breakdown of a round variable density jet, *J. Fluid Mech.*, 249, p.619, 1993
28 Cetegen, B. M., Behavior of naturally unstable and periodically forced axisymmetric buoyant plumes of helium and helium-air mixtures, *Phys. Fluids*, 9, p.3742-3752, 1997
29 Cetegen, B. M. and McTeague, J., Behavior of periodically forced buoyant plumes, in *Proc. Ann. Conf. on Fire Research*, (Eds), , 1996
30 Cetegen, B. M., Measurements of instantaneous velocity field of a non-reacting pulsating buoyant plue by Particle Image Velocimetry, *Combust. Sci. Technol.*, 123, p.377, 1997
31 Mell, W. E., Johnson, A., McGrattan, K. B. and Baum, H. R., Large eddy simulations of buoyant plumes, in *Chemical & Physical Processes in Combustion, Proc. Fall Technical Meeting*, (Eds), , 1995
32 Mell, W. E., McGrattan, K. B. and Baum, H. R., Numerical simulation of combustion in fire plumes, in *26th Symp. on Combustion*, (Eds), , 1996
33 Yep, T.-W., Agrawal, A. K. and Griffin, D., Gravitational effects on near-field flow structure of low-density gas jets, *AIAA J.*, 41, p.1973-1979, 2003
34 Pasumarthi, K. S. and Agrawal, A. K., Buoyancy effects on flow transition in low-density inertial gas jets, *Experiments in Fluids*, 38, p.541-544, 2005
35 Pera, L. and Gebhart, B., On the stability of laminar plumes: some numerical solutions and experiments, *Int. J. Heat Mass Transfer*, 14, p.975-984, 1971
36 Gebhart, B., Instability, transition and turbulence in buoyancy-induced flows, *Annu. Rev. Fluid Mech.*, 5, p.213, 1973
37 O'Hern, T. J., Tieszen, S. R., Weckman, E. J., Gerhart, A. L. and Schefer, R. W., Simultaneous cinematographic PIV and acetone PLIF for spatially and temporally resolved velocity and concentration fields in a buoyant helium plume, in *Proc. ASME Int. Mech. Eng. Congress & Exposition*, (Eds), , 2001
38 Nicolette, V. F., Tieszen, S. R., Black, A. R., Domino, S. P. and O'Hern, T. J., A turbulence model for buoyant flows based on vorticity generationS, in *Sandia Report SAND2005-6273*, (Eds), , 2005
39 Chung, W. and Devaud, C. B., Buoyancy-corrected k-epsilon models and large eddy simulation applied to a large axisymmetric helium plume, *Int. J. Num. Meth. Fluids*, 58, p.57-89, 2008
40 Blanquart, G. and Pitch, H., Large-eddy simulation of a turbulent buoyant helium plume, *Center for Turbulence Research*, Annual Research Briefs, p.245-252, 2008
41 Burton, G. C., Large-eddy simulation of a turbulent helium-air plume using the nLES method, *Center for Turbulence Research*, Annual Research Briefs, p.261-271, 2009
42 Tieszen, S. R., Domino, S. P. and Black, A. R., Validation of a simple turbulence model suitable for closure of temporally-filtered Navier-Stokes equations using a helium plume, in *Sandia Report SAND2005-3210*, (Eds), , 2005
43 Lingens, A., Neemann, K., Meyer, J. and Schreiber, M., Instability of diffusion flames, in *Proc.*

26th Symposium (International) on Combustion, (Eds), The Combustion Institute, Pittsburgh, PA, 1996
44 Lingens, A., Reeker, M. and Schreiber, M., Instability of buoyant diffusion flames, *Exp. Fluids*, 20, p.241-248, 1996
45 Zhou, X., Luo, K. H. and Williams, J. J. R., Large-eddy simulation of a turbulent forced plume, *Eur. J. Mech. B - Fluids*, 20, p.233-254, 2001
46 Zhou, X., Luo, K. H. and Williams, J. J. R., Study of density effects in turbulent buoyany jets using large-eddy simulation, *Theoret. Comput. Fluid Dynamics*, 15, p.95-120, 2001
47 George, W. K. Jr., Alpert, R. L. and Tamanini, F., Turbulence measurements in an axisymmetric buoyant plume, *Int. J. Heat Mass Transfer*, 20, p.1145-1154, 1977
48 Shabbir, A. and George, W. K., Experiments on a round turbulent buoyant plume, *J. Fluid Mech.*, 275, p.1-32, 1994
49 Zhou, X. and Hitt, D. L., Proper orgthonal decomposition analysis of coherent structures in a transient buoyant jet, *J. Turbulence*, 5, p.1-21, 2004
50 Pham, M. V., Plourde, F. and Doan, S., Direct and large-eddy simulations of a pure thermal plume, *Phys. Fluids*, 19, p.DOI: 10.1063/1.2813043, 1997
51 Meneveau, C., Lund, T. and Cabot, W., A Lagrangian dynamic subgrid-scale model of turbulence, *J. Fluid Mech.*, 319, p.353-385, 1996
52 Worthy, J. and Rubini, P. A., Large eddy simulation of buoyant plumes, in *Proc. 4th Int. Seminar on Fire & Explosion Hazards*, (Eds), , 2003
53 Worthy, J. and Rubini, P., A study of LES stress and flux models applied to a buoyant jet, *Num. Heat Trans. Part B*, 48, p.235-256, 2005
54 Worthy, J., *Large eddy simulation of buoyant plumes*, , School of Mech. Eng, Cranfield University, UK 2003
55 Metais, O. and Lesieur, M., Spectral large eddy simulations of isotropic and stably-stratified turbulence, *J. Fluid Mech.*, 239, p.157, 1992
56 Schumann, U., Subgrid-scale model for finite-difference simulations in plane channels and annuli, *J. Comp. Phys.*, 18, p.376, 1975
57 Leonard, A., Energy cascade in large-eddy simulations of turbulent flows, *Adv. Geophys.*, 18, p.237, 1974
58 Bardina, J., Ferziger, J. H. and Reynolds, W. C., Improved subgrid scale models for large eddy simulations, in *AIAA Paper 80-1357*, (Eds), , 1980
59 Burton, G. C. and Dahm, W. J., Multifractal subgrid-scale modeling for large eddy simulation. Part I: Model development and a priori testing, *Phys. Fluids*, 17, p.075111, 2005
60 Burton, G. C. and Dahm, W. J., Multifractal subgrid-scale modeling for large eddy simulation. Part II: Backscatter limiting and a posteriori evaluation, *Phys. Fluids*, 17, p.075112, 2005
61 Kang, Y. and Wen, J. X., Large eddy simulation of a small pool fire, *Combust. Sci. and Tech.*, 176, p.2193-2223, 2004
62 Wen, J. X., Kang, K., Donchev, T. and Karwatzki, J. M., Validation of FDS for the prediction of medium-scale pool fires, *Fire Safety Journal*, 42, p.127-138, 2007
63 Bastiaans, R. J. M., Rindt, C. C. M., Nieuwstadt, F. T. M. and van Steenhoven, A. A., Direst and large-eddy simulation of the transition of two and three-dimensional plane plumes in a confined enclosure, *Int. J. Heat Mass Transfer*, 43, p.2375-2393, 2000
64 Blanchat, T. K., Characterization of the air source and plume source at FLAME, in *SAND2001-2227*, (Eds), , 2001
65 Germano, M., Piomelli, U., Moin, P. and Cabot, W. H., A dynamic subgrid scale eddy viscosity model, *Phys. Fluids A*, 3, p.1760, 1991
66 Lilly, D. K., A proposed modification to the Germano subgrid-scale closure model, *Phys. Fluids A*, 4, p.663, 1992
67 Fureby, C., On subgrid scale modelling in large eddy simulations of compressible flow, *Phys.*

Fluids, 8, p.101, 1996
68 Ragab, S. A. and Sheen, S., Large eddy simulation of a mixing layer, in *AIAA Paper 91-0233*, (Eds), , 1991
69 Ragab, S. A., Sheen, S. and Sreedhar, M., An investigation of finite difference methods for large eddy simulations of a mixing layer, in *AIAA Paper 92-0554*, (Eds), , 1992
70 O'Rourke, P. J. and Bracco, F. V., Two scaling transformations for the numerical computation of multidimensional unsteady laminar flames, *J. Comput. Phys.*, 33, p.184, 1979
71 Ramshaw, J. D., O'Rourke, P. J. and Stein, L. R., Pressure gradient scaling method for fluid dlow with nearly uniform pressure, *J. Comput. Phys.*, 58, p.360, 1985
72 Rudy, D. H. and Strikwerda, J. C., A nonreflecting outflow boundary condition for subsonic Navier-Stokes calculations, *J. Comput. Phys.*, 36, p.55-70,
73 Rudy, D. H. and Strikwerda, J. C., Boundary-conditions for subsonic compressible Navier-Stokes calculations, *J. Comput. Phys.*, 9, p.327-338, 1981
74 Ghosal, S., An analysis of numerical errors in large-eddy simulations of turbulence, *J. Comp. Phys.*, 125, p.187-206, 1996
75 Mittal, R. and Moin, P., Suitability of upwind-biased finite difference schemes for large-eddy simulation of turbulent flows, *AIAA J.*, 35, p.1415-1417, 1997
76 Pierce, C. D., *Progress-variable approach for large eddy simulation of combustion*, , Dept. of Mech. Eng., Stanford University, California 2001
77 Pierce, C. D. and Moin, P., Progress-variable approach for large eddy simulation of non-premixed turbulent combustion, *J. Fluid Mech.*, 504, p.73-97, 2004
78 McGrattan, K., Fire Dynamics Simulator (Version 4): Technical Reference Guide, in *NIST Special Publication 1018*, (Eds), , 2006
79 Geurts, B. J. and Frohlich, J., Numerical effects contaminating LES: a mixed story, in *Modern simulation strategies for turbulent flow*, B. J. Geurts (Eds), R. T. Edwards Inc., 2001
80 Ferziger, J. H. and Peric, M., *Computational Methods for Fluid Dynamics*, Springer-Verlag, Berlin,2004
81 Geurts, B. J., Interacting errors in large-eddy simulation: a review of recent developments, *J. Turbulence*, 7, p., 2006
82 Boris, J. P., Grinstein, F. F., Oran, E. S. and Kolbe, R. L., New insights into Large Eddy Simulation, *Fluid Dyn. Res.*, 10, p.199-228, 1992
83 Pope, S. B., Ten questions concerning the large-eddy simulation of turbulent flows, *New Journal of Physics*, 6, p.1-24, 2004
84 Gullbrand, J. and Chow, F. K., The effect of numerical errors and turbulence models in large-eddy simulations of channel flow, with and without explicit filtering, *J. Fluid Mech.*, 495, p.323-341, 2003
85 Geurts, B. J., *Elements of direct and large-eddy simulation*, R. T. Edwards, ,2003
86 Meyers, J., Geurts, B. J. and Baelmans, M., Optimality of the dynamic procedure for large-eddy simulation, *Phys. Fluids*, 17, p.045108, 2005
87 Klein, M., An attempt to assess the quality of large eddy simulations in the context of implicit filtering, *Flow Turbulence and Combustion*, 75, p.131-147, 2005
88 Freitag, M. and Klein, M., An improved method to assess the quality of large eddy simulations in the context of implicit filtering, *J. Turbulence*, 7, p., 2006
89 Celik, I. B., Klein, M., Freitag, M. and Janicka, J., Assessment measures for URANS/DES/LES: an overview with applications, *J. Turbul.*, doi:10.1080/14685240600794379, p., 2006
90 Celik, I, Klein, M. and Janicka, J., Assessment measures for engineering LES applications, *J. Fluids Eng.*, doi:10.1115/1.3059703, p., 2009
91 Gant, S. E., Reliability issues of LES-related approaches in an industrial context, *Flow, Turb. Combust.*, 84, p.325, 2009

92 Baggett, J. S., Jimenez, J. and Kravchenko, A. G., Resolution requirements in large-eddy simulations of shear flows, in *Annual Research Briefs, Center for Turbulence Research, Stanford*, (Eds), , 1997
93 Addad, Y., Benhamadouche, S. and Laurence, D., The negatively buoyant wall-jet: LES results, *Int. J. Heat Fluid Flow*, 25, p.795-808, 2004